Universiteit Utrecht

Institute for Theoretical Physics

Master Thesis

Number Fluctuations and Phase Diffusion in a Bose-Einstein Condensate of Light

Author:
E.C.I. van der Wurff BSc

Supervisors:
A.-W. de Leeuw MSc
dr. R.A. Duine
prof. dr. ir. H.T.C. Stoof

September 2014

Abstract

Bose-Einstein condensates of quasiparticles such as exciton-polaritons, magnons and massive photons allow for new experimental possibilities as compared to the atomic Bose-Einstein condensates. In this Thesis we focus on a condensate of photons, first created at Bonn University in 2010. One of the recent achievements is the measurement of number fluctuations in such a condensate of photons. We present a general theory to calculate these number fluctuations in a harmonically trapped interacting Bose gas and apply this to the available experimental results on the condensate of photons, finding good quantitative agreement. Additionally, we investigate the fundamental phenomenon of phase diffusion, which is based on the fact that a Bose-Einstein condensate can be described as a symmetry-broken phase. However, the symmetry-broken phase is only well defined in the thermodynamic limit, such that in a finite system the phase of the Bose-Einstein condensate can have nontrivial dynamics. We propose a new type of interference experiment involving a condensate of photons to measure this dynamical behavior of the phase. By calculating the effects of quantum and thermal fluctuations we find different time scales on which the interference pattern vanishes. Based on these time scales, we conclude that phase diffusion is experimentally observable within the precision of current devices.

Contents

Nomenclature

Here we list all symbols we use throughout this Thesis, in alphabetic order.

Symbol	Definition	Units	Description
α	$-$	1	damping parameter for photons
β	$(k_B T)^{-1}$	J^{-1}	reciprocal temperature
c	c_{light}/n	$\mathrm{m{\cdot}s}^{-1}$	speed of light in medium with index of refraction n
δ	$\hbar(\omega_{\mathsf{cutoff}} - \omega_0)$	J	detuning dye
D_0	$-$	m	distance between centers of cavity mirrors
$D(\mathbf{x})$	$D_0 - 2(R - \sqrt{R^2 - \lvert\mathbf{x}\rvert^2})$	m	distance between cavity mirrors
D	$g/2\pi R_{\mathsf{TF}}^2$	J	diffusion constant Schrödinger equation phase
Δ	$-$	J	energy difference excited and ground state dye molecule
ϵ	$-$	K^{-1}	first-order correction to index of refraction
$\bar{\epsilon}$	M_{eff}/M	1	fitting parameter effective reservoir size
$\phi_0(\mathbf{x})$	$-$	m^{-1}	macroscopic 2D condensate wave function
g	$-$	$\mathrm{J{\cdot}m}^2$	photon-photon contact interaction
$\tilde{g}$	$mg/\hbar^2$	1	dimensionless interaction strength
g_{mol}	$-$	$\mathrm{J{\cdot}m}^{3/2}$	coupling constant photons and dye molecules
$g^{(2)}(t_1, t_2)$	$\frac{\langle N_0(t_1) N_0(t_2)\rangle}{\langle N_0(t_1)\rangle\langle N_0(t_2)\rangle}$	1	second-order correlation function
$g^{(2)}(0)$	$\langle N_0^2\rangle / \langle N_0\rangle^2$	1	zero-time delay autocorrelation function
Γ	$-$	s^{-1}	decay rate excited state dye molecules
$\mathbf{k_x}$	(k_x, k_y)	m^{-1}	transverse photon wavenumber

$\mathbf{k}_+$	$(0,0,k_z)$	m^{-1}	wavenumber of photons in the condensate
$\lambda_{\mathsf{cutoff}}$	$\hbar/mc$	m	cutoff wavelength cavity
μ	$-$	J	chemical potential
m	$\hbar k_z(0)/c$	kg	effective photon mass
M	$-$	kg	dye molecule mass
N_0	$-$	1	number of photons in condensate
$\langle N \rangle$	$-$	1	average number of photons in microcavity
N_c	$-$	1	critical particle number for condensation
n_{mol}	$-$	m^{-3}	density dye molecules in microcavity
n_{ph}	$-$	m^{-2}	density of photons in the microcavity
$\langle N_0^n \rangle$	$\int_0^\infty \mathrm{d}N_0 P(N_0) N_0^n$	1	n-th moment of the probability distribution
$P(N_0)$	$-$	1	probability distribution for N_0
q_{ho}	$\sqrt{\hbar/m\omega}$	m	harmonic oscillator length
q_{min}	$q_{\mathsf{ho}} \sqrt[4]{1+\tilde{g}N_0/2\pi}$	m	minimized variational parameter
R	$-$	m	radius of curvature of cavity mirrors
R_{TF}	$(4gN_0/\pi m\omega^2)^{1/4}$	m	Thomas-Fermi radius 2D trapped Bose gas
$\mathbf{r}$	(x,y,z)	m	three-dimensional position vector
σ	$-$	1	width Gaussian initial wave function
t_{col}	$5\hbar\sigma/2D$	s	time scale collapse quantum interference
t_{osc}	$\hbar/2DN_0$	s	time scale oscillation quantum interference
t_{rev}	$2\pi\hbar/D$	s	time scale revival quantum interference
$t_{\mathsf{dis}}^{(1)}$	$\hbar/4\alpha D N_0^2$	s	time scale collapse quantum interference with dissipation
$t_{\mathsf{dis}}^{(2)}$	$2\hbar\beta N_0/\alpha$	s	time scale collapse thermal interference
$V^{\mathsf{ext}}(\mathbf{x})$	$m\omega^2\lvert\mathbf{x}\rvert^2/2$	J	2D isotropic harmonic trapping potential
ω	$c\sqrt{2/D_0 R}$	s^{-1}	isotropic harmonic trapping frequency
ω_{cutoff}	$mc^2/\hbar$	s^{-1}	cavity cutoff frequency
ω_0	$-$	s^{-1}	dye-specific zero-phonon frequency
x	$\langle N_0 \rangle / \langle N \rangle$	1	condensate fraction
$\mathbf{x}$	(x,y)	m	two-dimensional transverse vector

Chapter 1

Introduction

Research on Bose-Einstein condensation has been an extremely active field of study in physics for almost two decades, both experimentally and theoretically. Since its first theoretical proposal by Bose [1] and Einstein [2] in the years 1924-1925, it took seventy years for the first weakly-interacting Bose-Einstein condensate to be created experimentally. Only after the development of advanced experimental techniques like laser cooling and evaporative cooling, the first condensates in weakly interacting dilute atomic alkali gases were observed in 1995. Almost simultaneously, three experimental groups created a condensate in atomic vapors of ^{87}Rb [3], ^{7}Li [4] and ^{23}Na [5]. The reason that these condensates were so hard to create, is that condensation in atomic gases only occurs at extremely low temperatures. In the case of a vapor of ^{87}Rb-atoms, the experimentalists cooled the gas down to a mind-boggling 170 nK.

In recent years, Bose-Einstein condensates of bosonic quasiparticles have also been created, such as an exciton-polariton condensate in 2006 [6, 7], a magnon condensate in 2006 [8] and a condensate of photons in 2010 [9]. These condensates of quasiparticles are realized under different circumstances compared to the atomic condensates. For instance, the condensates are created at higher temperatures than the condensates of dilute atomic gases: from several Kelvin for the exciton-polariton condensate to room temperature for the photonic condensate. Additionally, the condensates of quasiparticles are not in true equilibrium, since the steady state is a dynamical balance between particle losses and particle gain by external pumping with a laser. Due to these differences, new experimental possibilities have opened up. For example, large number fluctuations of the order of the total particle number have been observed in a condensate of photons [10].

In this Thesis we focus on condensates of photons. For a long time it was believed that photons could not undergo Bose-Einstein condensation. An illustration of this belief can be found in the clas-

sical textbook on statistical mechanics by K. Huang [11]: *"Bose-Einstein condensation can only occur when the particle number is conserved. For example, photons cannot condense. They have a simpler alternative, namely, to simply disappear in the vacuum."*. The reasoning behind this statement is that for blackbody radiation, which is a thermal gas of photons in free space, the number of photons N and the temperature of the gas T are related via $N \propto T^3$. This prevents the onset of Bose-Eintein condensation, because upon lowering the temperature of the system, the amount of photons also decreases.

Thus, in order to create a Bose-Einstein condensate of photons, one needs to find a so-called *number-conserving thermalization process*, by which the temperature and the photon number can be changed independently. The first suggestion of such a process was made in 1969, when Compton scattering of photons within a totally ionized plasma was considered [12]. It was shown that Bose-Einstein condensation occurs only when the absorption of the photons is negligible. However, in realistic experimental situations the absorption is not negligible in such a system, preventing the onset of Bose-Einstein condensation. A different route was followed in the years 1999-2001. In Refs. [13, 14, 15, 16] Chiao *et al.* consider a photon gas in a nonlinear Fabry-Pérot cavity. Due to the boundary conditions at the cavity walls, the photon gas becomes effectively two dimensional and the photons can be described by a dispersion relation similar to that of a massive boson. In this setup, thermalization is sought from photon-photon scattering due to the nonlinearity of the cavity. However, thermalization, a prerequisite for Bose-Einstein condensation, only occurs for sufficiently large nonlinearities. Unfortunately, the necessary magnitude of the nonlinearity cannot be reached experimentally and prevents the creation of a condensate in this type of system.

With some modifications, a similar experimental setup to the one proposed by Chiao *et al.* was used by the group of Martin Weitz at Bonn university to create the first condensate of photons in 2010. The main difference is the fact that the Fabry-Pérot cavity was filled with a solution of fluorescent dye molecules in an organic solvent. Thermalization of the photon gas is reached not by photon-photon scattering, but rather by multiple absorption and emission cycles of the photons by the fluorescent dye molecules [17]. It is this experimental setup, and the results obtained with it, that forms the starting point for the theoretical investigations in this Thesis.

1.1 Outline

We start in Chapter 2 by describing in detail the experimental set-up the physicists of Bonn University used to create the first condensate of photons. We also introduce some necessary theoretical concepts relevant for the condensate of photons. We proceed in Chapter 3 by considering the general case of a two-dimensional harmonically trapped gas of interacting bosons. For this system we calculate the probability distribution for the number of particles in a condensate by using a variational approach. We compare our results to the recent experimental results on a condensate of photons. Subsequently,

we discuss possible interaction mechanisms for the photons. In Chapter 4 we start by proposing a new type of interference experiment that can be done with the condensate of photons. The goal of the experiment is to measure phase diffusion. We also calculate typical interference patterns and estimate different timescales to investigate if it is experimental feasable to detect phase diffusion. Finally, we discuss the results from our research in Chapter 5. We also give an elaborate outlook on work in progress and what would be interesting to look at in the future.

Chapter 2

Bose-Einstein Condensation of Light

In this chapter we introduce the basic concepts for understanding the first experimental realization of Bose-Einstein condensation of photons by the group of M. Weitz at Bonn University in 2010. As already discussed in Chapter 1, the most challenging experimental task is to be able to independently tune the photon number and the temperature of the photon gas. We start by giving a general idea of the experimental scheme used by the Bonn group. We proceed by showing how the photons in the experimental setup can be described as quasiparticles with an effective mass. Subsequently, we explain the thermalization mechanism of the photon gas in depth. Hereafter, we calculate the minimal number of photons inside the cavity necessary for Bose-Einstein condensation to set in. Finally, we discuss experimental evidence for the condensation of photons. As an outlook to our theoretical description of the photon gas in the next chapter, we also show experimental results indicating that the photons are in fact interacting.[1]

2.1 Experimental Scheme

In the Bonn experiment photons are confined in an optical microcavity formed by two spherical mirrors, see Fig. 2.1a. Between these mirrors a solution is placed, consisting of an organic solvent (typically methanol or ethanol) and fluorescent dye molecules (typically Rhodamine 6G or perylene-diimide). By pumping the solution with an external laser photons are introduced into the cavity. These photons are repeatedly absorbed and re-emitted by the dye molecules, yielding thermal equilibrium between the dye solution and the photon gas. In section 2.3, we discuss in more detail how this leads to a number-conserving thermalization process.

[1] A lot of the material in this chapter is a revised version of the excellent articles by the Bonn group [9, 17, 18, 19, 20]. Here we give our personal take on their work.

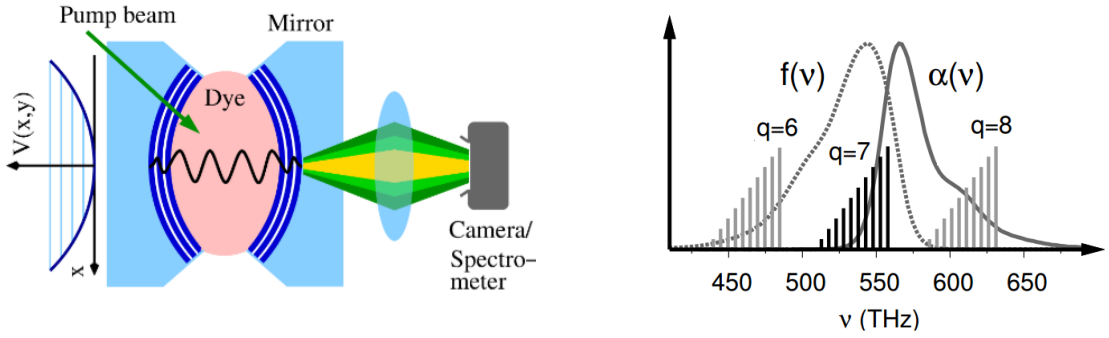

(a) Experimental scheme

(b) Cavity spectrum and absorption/fluorescence dye

Figure 2.1: Schematic image of the bispherical optical microcavity in Fig. (a). In Fig. (b) a sketch of the cavity modes is displayed. The multiplets corresponds to all modes with a fixed longitudinal mode of q and a variable transversal mode. Also, the absorption $\alpha(\nu)$ and fluorescence $f(\nu)$ spectrum of the dye molecules as a function of the frequency ν are shown. The multiplet with $q = 7$ (depicted in black) lies within both the absorption and the fluorescence spectrum of the dye molecules. Images taken from Ref. [9].

Furthermore, due to the boundary conditions imposed by the mirrors the longitudinal modes in the cavity are quantized. Additionally, the longitudinal modes in the resonator obtain a large frequency spacing because of the small spatial mirror separation (typically between 1 and 2 μm) in the longitudinal direction. In fact, this frequency spacing is of the order of the emission width of the dye molecules, such that the dye molecules can only absorb and emit photons of the same longitudinal mode. This is schematically displayed in Fig. 2.1b. Also, the spontaneous emission rate of the dye molecules is changed by the finite volume of the cavity, as compared to the rate in vacuum [21]. One can show that the spontaneous emission rate is modified to prefer emission of photons in the longitudinal direction, i.e., with relatively low transverse momenta [22]. In this manner the microcavity is approximately only populated by photons with one longitudinal mode. Therefore, in good approximation this mode is fixed and the gas of photons becomes effectively two dimensional.

In the next section we show how this confinement leads to a modified dispersion relation for the photons. In fact, the dispersion relation is altered from going linearly with momentum, to quadratically with momentum. This allows one to view the photons as particles with an effective mass.

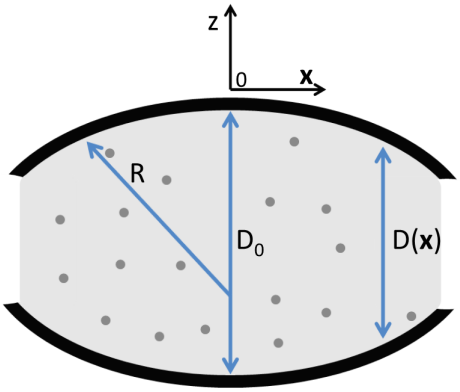

Figure 2.2: Schematic picture of the microcavity to indicate the relevant coordinate axes and symbols. The distance between the mirrors depends on the radial coordinate $\mathbf{x}$: $D(\mathbf{x})$. The distance between the two mirror centers is approximately $D_0 \simeq 1.46$ μm for a typical experiment. The image is not to scale, e.g. the curvature of the mirrors is actually $R \simeq 1$ m.

2.2 Massive Photons

To show how the dispersion relation for the photons becomes quadratic, we start by considering the standard energy-momentum relation for photons in a medium with a speed of light c, that is,

$$\epsilon(\mathbf{k}) = \hbar c|\mathbf{k}| = \hbar c\sqrt{k_z^2 + |\mathbf{k_x}|^2}, \tag{2.1}$$

where k_z denotes the longitudinal wavenumber of the photons and $\mathbf{k_x} = (k_x, k_y)$ is the transverse wavenumber of the photons. Assuming metallic boundary conditions for the two cavity mirrors, the photon field must vanish at the mirrors. By using elementary geometry one shows that the distance D between the mirrors depends on the radial direction $|\mathbf{x}| = \sqrt{x^2 + y^2}$ and is given by $D(\mathbf{x}) = D_0 - 2(R - \sqrt{R^2 - |\mathbf{x}|^2})$, where D_0 is the distance between the two centers of the mirrors and R denotes the radius of curvature of those mirrors. These quantities are schematically depicted in Fig. 2.2. To obtain a standing wave, as is necessary when one assumes metallic boundary conditions for the mirrors, the quantization condition on the longitudinal wavenumber becomes $k_z(\mathbf{x}) = q\pi/D(\mathbf{x})$, with $q \in \mathbb{N}_{>0}$.

In the paraxial limit the mirrors have a small separation in the longitudinal direction and a curvature which is much larger than the typical radial distance. This amounts to taking $k_z \gg |\mathbf{k_x}|$ and $|\mathbf{x}| \ll R$. Since typical experimental values are $D_0 \simeq 1.46$ μm and $R \simeq 1$ m, such that we can take the paraxial limit and we find for the longitudinal wavenumber

$$k_z(\mathbf{x}) = \frac{q\pi}{D_0 - 2(R - \sqrt{R^2 - |\mathbf{x}|^2})} \approx \frac{q\pi}{D_0}\left(1 + \frac{2|\mathbf{x}|^2}{D_0 R}\right), \tag{2.2}$$

such that we have $k_z(0) = q\pi/D_0$ at the center of the mirrors. Substituting Eq. (2.2) into Eq. (2.1) we find for the dispersion relation of the photons in the paraxial limit [9]

$$\begin{aligned}\epsilon(\mathbf{k}) &\approx \hbar c k_z(\mathbf{x})\left(1+\frac{|\mathbf{k}_\mathbf{x}|^2}{2k_z(\mathbf{x})^2}\right) \approx \hbar c k_z(0) + \frac{2\hbar c|\mathbf{x}|^2 k_z(0)}{D_0 R} + \frac{\hbar c|\mathbf{k}_\mathbf{x}|^2}{2k_z(0)} \\ &:= mc^2 + \frac{1}{2}m\omega^2|\mathbf{x}|^2 + \frac{\hbar^2|\mathbf{k}_\mathbf{x}|^2}{2m}, \end{aligned} \tag{2.3}$$

where we defined the characteristic trap frequency $\omega := c\sqrt{2/D_0 R}$ and the effective photon mass $m := \hbar k_z(0)/c$. With these definitions we have written the dispersion relation in the suggestive form of a dispersion relation for a massive particle in an isotropic two-dimensional harmonic trapping potential given by $V^{\text{ext}}(\mathbf{x}) = m\omega^2|\mathbf{x}|^2/2$. Furthermore, from Eq. (2.3) we obtain that the photons in the cavity have a minimal energy mc^2. This defines a cutoff frequency and cutoff wavelength for the cavity via the equalities $mc^2 = \hbar\omega_{\text{cutoff}} = hc/\lambda_{\text{cutoff}}$.

For typical experimental values we find $m \simeq 6.7 \cdot 10^{-36}$ kg, $\omega \simeq 8\pi \cdot 10^{10}$ s^{-1} and $\hbar\omega_{\text{cutoff}} = 2.1$ eV [9]. Note that the value for the effective photon mass is ten orders of magnitude smaller than the typical mass for the atoms used in experiments concerning Bose-Einstein condensation of dilute atomic gases. Therefore, contrary to dilute atomic gases, one does not have to go to extremely low temperatures to reach a phase space density of order unity. In fact, for realistic photon densities inside the microcavity, room temperature is enough to reach Bose-Einstein condensation.

Now that we have discussed how the photons in the microcavity acquire an effective mass, we explain in the next section how the temperature of the photon gas can be tuned independently from the number of photons. Additionally, we discuss how this leads to a fixed number of photons within the microcavity.

2.3 Number-Conserving Thermalization

The photons in the microcavity are repeatedly absorbed and emitted by the present dye molecules. To understand how this leads to thermalization, we must first consider the electronic stucture of the dye molecules. The dye molecules typically consist of many different atoms, giving them a complex electronic structure. In general, the molecules will have electronic levels, which are split into different sublevels with different energies due to the possible excitation of rotational and vibrational states of the dye molecule. In the literature this is often referred to as a *rovibrational* structure. Analogously to Ref. [19], we denote the set of lower electronic levels by S_0 and the set of excited electronic levels by S_1. A schematic picture of this structure is displayed in Fig. 2.3.

If a photon is absorbed by a dye molecule, an electron is excited from a state $\alpha \in S_0$ to a state

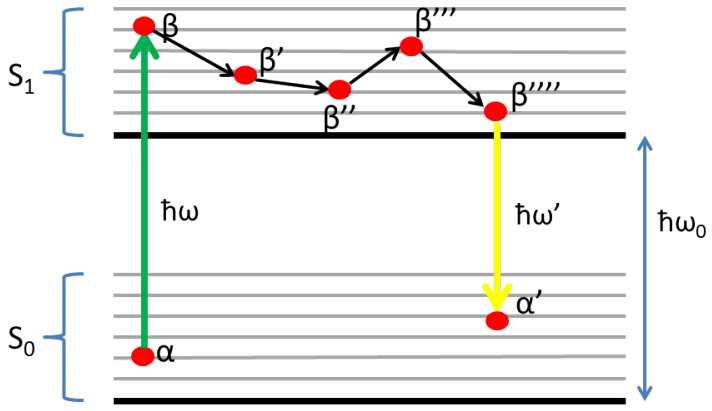

Figure 2.3: Schematic picture of the typical electronic structure of a dye molecule. The ground state (S_0) and excited state (S_1) are both split into sublevels. The energy difference between the lowest energy states of S_0 and S_1 is called the zero-phonon line and is denoted by $\hbar\omega_0$. The figure is based on a similar figure in Ref. [23].

$\beta \in S_1$. These excited states typically have a lifetime of the order of nanoseconds [17]. Whilst being in an excited state, the dye molecule undergoes collisions with solvent molecules on a femtosecond time scale. These collisions cause the electron to access different sublevels within the excited state, which is illustrated in Fig. 2.3 by the transition to the states β', β'' and so on. Due to the fast nature of these dye solvent collisions, the population of the rovibrational structure of the dye molecules is given by a thermal distribution at the temperature T of the solution. Subsequently, the thermal distribution of the solvent molecules is transferred to the photon gas via the dye molecules by multiple absorption and emission cycles. This leads to a thermalized distribution for the spectral distribution of the photon gas [23]. For a more precise mathematical treatment on this process using rate equations the reader is referred to Ref. [18].

Using the mechanism described above, the temperature of the photon gas in the microcavity can simply be changed by changing the temperature of the dye solution. Note that this process does not change the number of photons in the cavity. Indeed, the process allows for independent adjusting of the photon number and the temperature of the photon gas. Recall that this is in contrast to blackbody radiation, for which the number of photons N and temperature are inescapably linked via $N \propto T^3$.

Now that we have found a way to change the temperature of the photon gas, a mechanism to manipulate the number of photons in the cavity remains to be found. Firstly, note that the minimal energy of photons in the microcavity $\hbar\omega_{\text{cutoff}}$ is two orders of magnitude larger than the typical thermal energy of 25 meV. Therefore, photons cannot be created spontaneously by thermal fluctuations inside the microcavity, as is the case with blackbody radiation. Thus, after introducing photons into the microcavity with an external laser, the average number of photons remains fixed during the thermalization process. More photons can simply be added to the system by increasing the power of the external laser.

However, there is a small caveat: we treated the system ideally. In reality there are some losses of photons due to e.g. leaking through the mirrors because of an imperfect reflectivity and a finite quantum efficiency of the dye [23]. This is compensated for by carefully pumping with the external laser. In fact, the loss of photons by leaking through the mirrors yields a handy diagnostic tool. By analyzing the photons leaking through the mirrors, one can obtain information on what is happening inside the microcavity. This means that nondestructive measurements of the condensate inside the microcavity can easily be performed, contrary to the typical case in atomic condensates.

In the next section we calculate the critical particle number necessary for Bose-Einstein condensation to set in.

2.4 Critical Particle Number

In the previous two sections we have shown how thermalization is reached in the microcavity and that the photons in the optical microcavity can be described as quasiparticles with an effective mass in a two-dimensional harmonic trapping potential. We proceed by considering the necessary conditions for Bose-Einstein condensation of the photon gas. From quantum mechanics we know that the two-dimensional harmonic oscillator Hamiltonian can be solved independently in both directions to yield the quantum numbers n_x, $n_y \in \mathbb{N}$ and the corresponding energy[2]

$$\epsilon(n_x, n_y) = (n_x + n_y + 1)\hbar\omega = \epsilon_x + \epsilon_y + \hbar\omega. \tag{2.4}$$

For energies large compared to the ground state energy, we ignore the ground-state energy $\hbar\omega$ and consider the $\epsilon_i = n_i\hbar\omega$ to be continuous variables. The number of states available to particles with an energy less than $\epsilon = \epsilon_x + \epsilon_y$ is called $N(\epsilon)$ and is given by [24]

$$N(\epsilon) = \frac{N_s}{\hbar^2\omega^2}\int_0^{\epsilon} \mathrm{d}\epsilon_x \int_0^{\epsilon-\epsilon_x} \mathrm{d}\epsilon_y = \frac{N_s}{2}\left(\frac{\epsilon}{\hbar\omega}\right)^2, \tag{2.5}$$

where the integer N_s denotes the number of spin components of the boson. Note that the photons are described with an effective mass m, associated with their fixed longitudinal wavenumber. However, the effective nonrelativistic form of the Hamiltonian does not change the spin degeneracy for these photons inside the cavity. Thus, we still have $N_s = 2$, as is the case for 'ordinary' photons. The density of states $D(\epsilon)$ follows from taking the derivative of the number of available states

$$D(\epsilon) = \frac{\mathrm{d}N(\epsilon)}{\mathrm{d}\epsilon} = \frac{2\epsilon}{\hbar^2\omega^2}. \tag{2.6}$$

[2] In general the expression would read $\epsilon(n_x, n_y) = \hbar\omega_x(n_x + 1/2) + \hbar\omega_y(n_y + 1/2)$, but here it simplifies due to the isotropy of the harmonic trapping potential, i.e., $\omega_x = \omega_y = \omega$.

Note that we have $k_B T \gg \mu$, which implies that the thermal cloud around the condensate can be accurately described by a noninteracting thermal gas of bosons. This then implies that for temperatures T below the critical temperature for Bose-Einstein condensation, the average number of particles in excited states $\langle N_{\mathsf{ex}}(T)\rangle$ can be determined from the ideal-gas result for $\mu = 0$. We obtain

$$\langle N_{\mathsf{ex}}(T)\rangle = \int_0^\infty \frac{D(\epsilon)\,\mathrm{d}\epsilon}{\exp(\beta\epsilon) - 1} = \frac{1}{3}\left(\frac{\pi}{\hbar\beta\omega}\right)^2, \tag{2.7}$$

which determines the critical particle number N_c for a fixed temperature T by the relation $N_c = \langle N_{\mathsf{ex}}(T)\rangle$. This means that if we keep the temperature fixed and increase the number of particles beyond this critical particle number, the excess particles start occupying the ground state. Hence, a Bose-Einstein condensate forms if the number of particles in the system is larger than N_c. For a typical trap frequency $\omega \simeq 8\pi \cdot 10^{10}$ and temperature $T = 300$ K, we obtain a critical particle number of $N_c \approx$ 77,000.

Finally, note that the two-dimensional harmonic trapping potential in the effective dispersion relation Eq. (2.3) is crucial for Bose-Einstein condensation to occur in the two-dimensional gas of photons. Indeed, for a homogeneous gas of bosons confined to an area A, i.e., without a trapping potential, the density of states is a constant: $D(\epsilon) = Am/\pi\hbar^2$ [24]. The critical particle number at a fixed temperature T is then equal to

$$N_c = \frac{Am}{\pi\hbar^2}\int_0^\infty \frac{\mathrm{d}\epsilon}{\exp(\beta\epsilon) - 1}, \tag{2.8}$$

which diverges due to the pole at $\epsilon = 0$. Thus, the critical particle number is infinite and Bose-Einstein condensation cannot occur at a finite temperature. Hence, the harmonic trapping potential in Eq. (2.3) gives the photon gas the possibility to condense.

In the next section we briefly discuss how the critical particle number for the onset of condensation is reached inside the microcavity. Additionally, we show experimental evidence for the phase transition of the photon gas to a Bose-Einstein condensate of photons.

2.5 Experimental Evidence for Photon Condensation

In order for a condensate of photons to appear in the microcavity, one has to increase the number of photons in the cavity above the critical particle number. This is done by increasing the power of the external pump laser. However, one cannot simply keep increasing the pumping power, as the energy dissipated in the system increases accordingly. This would induce heat development, possibly changing the optical properties of the system.[3] Therefore, the laser light is acousto-optically chopped to

[3] In fact, in Subsection 3.7.1 we argue that the index of refraction of the dye solution is altered due to a change in temperature and estimate a corresponding effective photon-photon interaction due to temperature fluctuations. This

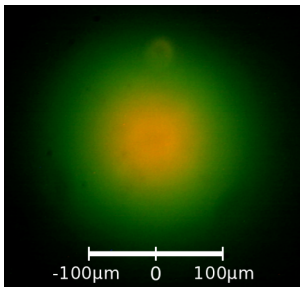

(a) Below the critical particle number

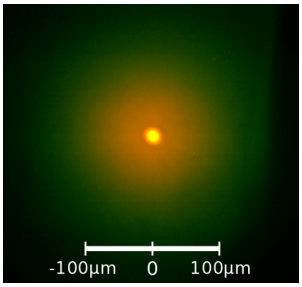

(b) Above the critical particle number

Figure 2.4: Images of the radiation emitted along the cavity axis that leaks through the cavity mirrors. The images are made by the sensor of a color CCD camera. As the pumping power of the external laser is increased from below [Fig. (a)] to above [Fig. (b)] the critical pumping power, the number of photons in the cavity becomes larger than the critical particle number of $N_c \approx 77,000$ and a condensate peak becomes visible in the center. Images taken from Ref. [9].

0.5-μm pulses, with a repetition time of several milliseconds. It is important to note that the lifetime of the excited states of the dye molecules is two orders of magnitude smaller than the pulse duration. Additionally, the lifetime of the photons in the cavity is four orders of magnitude smaller than the pulse duration. Due to these large differences in time scales, the experiment is effectively performed in a quasistatic regime [18].

In Fig. 2.4 we show two typical images of the light that leaks out of the microcavity onto the CCD camera. The images depict the radiation that is emitted along the longitudinal cavity axis. Hence, the radiation falling exactly onto the center of the CCD camera corresponds to photons with zero transversal wavenumber which are in the ground state of the system. On the other hand, photons with a nonzero transversal wavenumber are emitted at an angle to the optical axis. Due to their higher total wavenumber, the latter photons have a higher energy, resulting in a blueshift of the color of the radiation from yellow to green. Fig. 2.4a depicts a typical image for a pumping power below the critical pumping power. In this case we see a smooth transition from yellow radiation in the center to green radiation off-center. When the power is increased above the critical pumping power, an image like Fig. 2.4b appears on the CCD camera. We see that the intensity of the yellow light in the center of the image has increased dramatically, which is interpreted as a macroscopic occupation of the ground state of the system. Furthermore, the transition from yellow to green radiation is more abrupt. This is a qualitative visual indication that a Bose-Einstein condensate of photons has formed.

More quantitative evidence for the onset of condensation of photons is depicted in Fig. 2.5. The spectral photon distribution as a function of the wavelength of the light is displayed for increasing intracavity powers in Fig. 2.5a. The light power in the cavity is determined by measuring the transmitted power through the mirrors. With a separately measured transmission coefficient for the mirror, one

change in temperature can be caused by overpumping with the external laser.

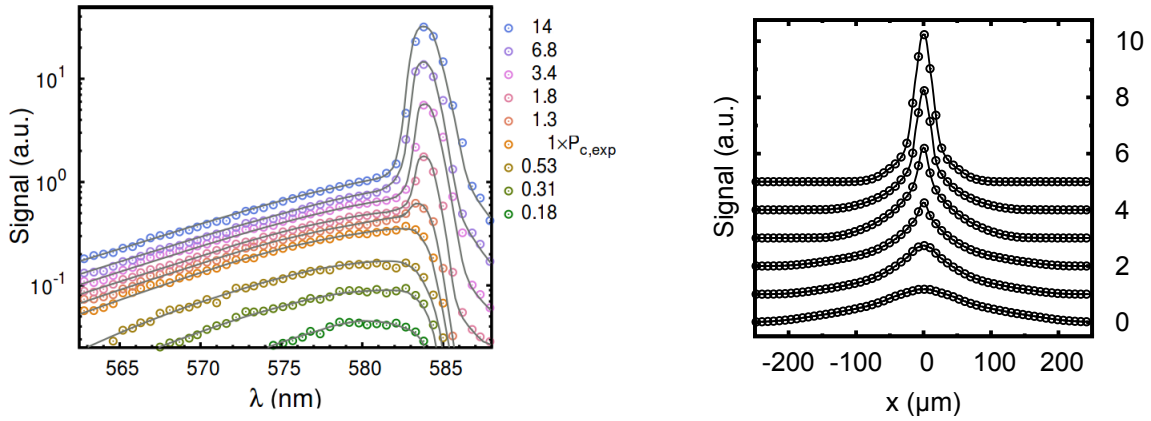

(a) Spectral photon distributions

(b) Spatial photon distributions

Figure 2.5: Experimental signatures of the onset of condensation of photons. Fig. (a) depicts the spectral photon distribution in arbitrary units as a function of the wavelength of the light for increasing intracavity power. The optical powers are normalized to the experimentally determined critical power $P_c = (1.55 \pm 0.60)$ W. Above the critical power the signal becomes highly peaked around a wavelength associated with the transverse ground-state energy. Fig. (b) shows the spatial photon distribution in arbitrary units along an axis intersecting the trap center as a function of the distance from that center. The lowest curve corresponds to a condensate fraction of 0% and the highest to a fraction of about 25%. Note that the curves are shifted upwards by hand for clarity. The images are revised versions from images in Refs. [9, 18].

can then calculate the power inside the cavity. For low intracavity powers we observe a Boltzmann distribution for the spectral distribution. As the intracavity power is increased, the maximum of the distribution shifts to higher wavelengths. Above a certain critical pumping power, a narrow peak in the spectral distribution appears around the cutoff wavelength. Upon increasing the power even further, the peak increases in height. This behavior is again a signature for the onset of Bose-Einstein condensation of the photons. Additionally, the critical pumping power is experimentally determined to be $P_c = (1.55 \pm 0.60)$ W. With this, one can estimate the critical photon number in the cavity by considering the power per photon. This yields $N_c = (6.3 \pm 2.4) \cdot 10^4$ [9], which is consistent with the critical particle number we estimated by using Eq. (2.7). Interestingly, the critical particle number was experimentally determined to be roughly the same for a dye solution of Rhodamine 6G in methanol and a solution of perylene-diimide in aceton. This is to be expected, as Eq. (2.7) is only a function of the trapping frequency ω and independent of the properties of the dye.

Furthermore, we show spatial photon distributions in Fig. 2.5b. These were obtained by recording images like those in Fig. 2.4 for different intracavity powers. Note that the curves in the figure are shifted upwards for visual clarity. We see that the intensity of the transmitted light at the center of the spot on the CCD camera increases drastically upon increasing the pumping power, again indicating the phase transition to a condensate of photons.

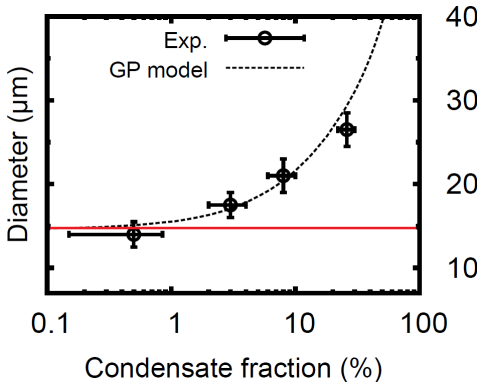

Figure 2.6: Plot of the condensate diameter in μm against the condensate fraction in percentages. The red line depicts the result expected when the photons do not interact. The included experimental data points in the figure are fitted to a numerical solution of a Gross-Pitaevskii equation with a nonzero photon-photon interaction strength g. The figure is a revised version of an image in Ref. [9].

Finally, we observe in Fig. 2.5b that the width of the condensate increases for the increasing condensate fractions corresponding to higher intracavity powers. This is evidence for the existence of repulsive interactions between the photons in the microcavity. As this will be crucial for our theoretical treatment of number fluctuations in the photon condensate in the next chapter, we discuss this in more detail in the next section.

2.6 Interaction Effects

Klaers *et al.* systematically measured the diameter of the photonic condensate as a function of its condensate fraction, as is shown in Fig. 2.6. In these measurements, the condensate diameter is defined as the full width at half maximum of the condensate density. We see that if the condensate fraction, and thus the number of photons in the condensate, is increased, also the diameter of the condensate increases. There is an intuitive explanation for this in terms of interactions between the photons in the condensate.

If there were no interaction between the photons, we would simply expect the condensate diameter to be constant as a function of the condensate fraction. Namely, in the case of a harmonically trapped gas of ideal bosons, the exact condensate density is a Gaussian [24]. The characteristic decay length for this Gaussian is the harmonic oscillator length $q_{\mathrm{ho}} = \sqrt{\hbar/m\omega}$. The corresponding condensate diameter is twice this value and indicated by a red line in Fig. 2.6. Note that for small condensate fractions the diameter should approach this value (as it does in the figure), because highly dilute gases can be treated as noninteracting. On the other hand, we can consider the case of repulsive interactions between the photons. Say we add particles to the condensate. Due to the repulsive interactions, the

particles will increase their separation to lower the total interaction energy. This implies that the condensate grows in size when the condensate fraction increases. This is exactly the behavior we deduce from the experimental results in Fig. 2.6.

These considerations motivated Klaers *et al.* to fit the results to a numerical solution of the Gross-Pitaevskii equation [9]. This famous equation is well known and accurately describes the dynamics of a Bose-Einstein condensate at sufficiently low temperatures. In the case of a harmonic trapping potential with frequency ω its time-independent variant reads

$$\left(-\frac{\hbar^2\nabla^2}{2m}+\frac{1}{2}m\omega^2|\mathbf{x}|^2-\mu+g|\phi_0(\mathbf{x})|^2\right)\phi_0(\mathbf{x})=0, \tag{2.9}$$

where $\phi_0(\mathbf{x})$ is the macroscopic wave function of the condensate, μ is the chemical potential of the system and the last term represents a contact interaction between the photons with a strength g. Solving this differential equation for $\phi_0(\mathbf{x})$ for a fixed value of g and subsequently calculating the corresponding diameter of the condensate, the dashed curve in Fig. 2.6 was obtained. We observe good agreement, indicating that interactions between the photons are crucial in order to explain experimental results. Finally, note that the fact that these experimental results can be modelled accurately with the Gross-Pitaevskii equation is another proof that the photons have indeed formed a condensate.

2.7 Conclusion

In this chapter we have explained recent experimental endeavors to create a Bose-Einstein condensate of light. The main experimental difficulty was to find a number-conserving thermalization process, i.e., a way to tune the number of photons in the system and the temperature of the photon gas independently. We explained that this is possible by confining photons in a dye-filled microcavity. The photons in the cavity behave like particles with an effective mass in a harmonic trapping potential, such that they are quasiparticles. The most promising aspect of the experimental setup is that measurements can be performed without destroying the condensate: one simply measures the photons leaking from the cavity mirrors and performs analysis on this signal.

Chapter 3

Number Fluctuations in a Condensate of Light

In this chapter we investigate number fluctuations in Bose-Einstein condensates. We variationally obtain an equilibrium probability distribution for the number of particles in a condensate by introducing an effective contact interaction into the grand-canonical Hamiltonian of a generic Bose gas. Subsequently, we proceed by investigating these distributions for different condensate fractions and interaction strengths and compare them to experimental results on a condensate of photons. We also calculate the zero-time delay autocorrelation function $g^{(2)}(0)$ to quantify the number fluctuations and compare this again to the experiments on photonic condensates. In both cases we find good quantitative agreement. Finally, we discuss possible microscopic mechanisms for the photon-photon interaction.

The contents of this chapter have been accepted for publication in the Physical Review Letters as *"Interaction Effects on Number Fluctuations in a Bose-Einstein Condensate of Light"*, E.C.I. van der Wurff, A.-W. de Leeuw, R.A. Duine and H.T.C. Stoof.

3.1 Introduction

Fluctuations are ubiquitous in physics: from the primordial quantum fluctuations in the early universe that reveal themselves as fluctuations in the cosmic microwave background, to current fluctuations in every-day conductors. For large voltages, the latter fluctuations give rise to shot noise, that is due to the discrete nature of charge [25]. As a consequence, shot noise can be used to determine the quanta of the electric charge of the current carriers in conducting materials [26]. Indeed, it has been used to characterize the nature of Cooper pairs in superconductors [27] and the fractional charge of the

quasiparticles of the quantum Hall effect [28]. For low voltages, the noise in the current is thermal and is called Johnson-Nyquist noise [29, 30]. Contrary to shot noise, thermal noise is always present in electrical circuits, even if no externally applied voltage is present, since it is due to thermal agitation of charge carriers, that leads to fluctuating electromotive forces in the material.

Theoretically, fluctuations in equilibrium are described by the fluctuation-dissipation theorem, as formulated by Nyquist in 1928 and proven decades later [31]. This theorem relates the response of a system to an external perturbation to the fluctuations in the system in the absence of that perturbation. Given a certain fluctuation spectrum we can reconstruct the response of the system. Therefore, this theorem is very powerful, as was fervently argued by the Japanese physicist Kubo [32].

Having stressed the importance of fluctuations in physics and the information they contain, we now zoom in on condensate-number fluctuations as our main point of interest. Traditionally, weakly interacting Bose-Einstein condensates were first observed in dilute atomic vapors [3, 4, 5]. For these systems, it is very difficult to measure number fluctuations because typically number measurements are destructive. Therefore, theoretical work has focused more on density-density correlation functions [33, 34]. However, with to the creation of the condensate of photons, new experimental possibilities have opened up. For example, large number fluctuations of the order of the total particle number have been predicted and observed in a photonic condensate [10, 20], which drew quite some attention [35]. In this chapter we investigate these number fluctuations in a two-dimensional harmonically trapped gas of interacting bosons. We start by calculating the probability distribution for the number of particles in the condensate in the next section.

3.2 Particle Number Probability Distribution

We consider a harmonically trapped Bose gas with a fixed number of particles. Because condensates of quasiparticles are typically confined in one direction, we specialize to the case of two dimensions. However, the following treatment is completely general and can easily be generalized to higher or lower dimensions.

To investigate the number fluctuations, we need to calculate the average number of particles $\langle N_0 \rangle$ in the condensate. Because condensates of quasiparticles allow for a free exchange of bosons with an external medium we treat the system in the grand-canonical ensemble: the probability distribution $P(N_0)$ for the number of condensed particles is of the form $P(N_0) \propto \exp[-\beta\Omega(N_0)]$, with $\Omega(N_0)$ the energy functional of the gas of bosons and $\beta := (k_B T)^{-1}$ the reciprocal temperature. To find the grand potential we use a variational wave function approach. We note that the bosons in the condensate typically interact with each other. Indeed, the experimental results on the diameter of the photonic condensate as a function of the condensate fraction shown in Section 2.6 indicate that the

photons exhibit nonnegligible repulsive interactions. A reasonable first approximation for the form of this interaction is a contact interaction, as essentially every interaction is renormalized to a contact interaction at long length and time scales, independent of the precise origin of the interaction.

Therefore, we consider the following energy functional for the macroscopic wave function $\phi_0(\mathbf{x})$ of the Bose-Einstein condensate [36]

$$\Omega[\phi_0(\mathbf{x})] = \int \mathrm{d}\mathbf{x}\left[\frac{\hbar^2}{2m}\left|\nabla\phi_0(\mathbf{x})\right|^2 + V^{\mathsf{ex}}(\mathbf{x})\left|\phi_0(\mathbf{x})\right|^2 - \mu|\phi_0(\mathbf{x})|^2 + \frac{g}{2}\left|\phi_0(\mathbf{x})\right|^4\right], \tag{3.1}$$

with $\mathbf{x}$ is the two-dimensional position, the first term represents the kinetic energy of the condensate, $V^{\mathsf{ex}}(\mathbf{x}) = m\omega^2|\mathbf{x}|^2/2$ is the harmonic trapping potential, μ is the chemical potential for the particles and g is the coupling constant of the effective pointlike interaction between the particles. Note that if we vary the energy functional with respect to the field $\phi_0^*(\mathbf{x})$, we exactly obtain the Gross-Pitaevskii equation Eq. (2.9) which was used to successfully model the increase of the condensate diameter as a function of the condensate fraction in Section 2.6.

We use the Bogoliubov substitution $\phi_0(\mathbf{x}) = \sqrt{N_0}\psi_q(\mathbf{x})$, with the normalized variational wave function $\psi_q(\mathbf{x})$, such that $\int \mathrm{d}\mathbf{x}|\phi_0(\mathbf{x})|^2 = N_0$. Subsequently, we minimize the energy as a function of the variational parameter q, which describes the width of the condensate. As an ansatz we take the variational wave function to be the Gaussian $\psi_q(\mathbf{x}) = (\sqrt{\pi}q)^{-1}\exp\left(-|\mathbf{x}|^2/2q^2\right)$. Substituting this into the energy given by Eq. (3.1) we obtain

$$\Omega_q = \frac{\hbar^2 N_0}{2mq^2} + \frac{1}{2}m\omega^2 N_0 q^2 + \frac{gN_0^2}{4\pi q^2}. \tag{3.2}$$

Minimizing this last expression with respect to the variational parameter, we find

$$q_{\mathsf{min}} = \sqrt[4]{\frac{2\pi\hbar^2 + mN_0 g}{2\pi\omega^2 m^2}} = q_{\mathsf{ho}}\sqrt[4]{1 + \frac{\tilde{g}N_0}{2\pi}}, \tag{3.3}$$

where we defined the dimensionless coupling constant $\tilde{g} := mg/\hbar^2$ and the harmonic oscillator length $q_{\mathsf{ho}} = \sqrt{\hbar/m\omega}$. Note that for a sufficiently small number of condensate particles q_{min} reduces to q_{ho}. This is to be expected: for a small number of particles interactions become negligible and the gas behaves as an ideal Bose gas in a harmonic trapping potential. It is well known that in this case the Schrödinger equation for the wave function of the condensate can be solved exactly and yields $\psi_{\mathsf{ho}}(\mathbf{x}) \propto \exp(-|\mathbf{x}|^2/2q_{\mathsf{ho}}^2)$ [24].

By substituting the minimal value for the variational parameter into the energy functional, we obtain the probability distribution for the number of particles in the condensate

$$P(N_0) \propto \ \exp\left[\beta N_0\left(\mu - \hbar\omega\sqrt{1 + \frac{\tilde{g}N_0}{2\pi}}\right)\right], \tag{3.4}$$

where the normalization is $\int_0^\infty \mathrm{d}N_0 P(N_0) = 1$. Experimentally, the relevant parameter is the condensate fraction $x := \langle N_0\rangle/\langle N\rangle$, with N the total number of particles. Thus, to relate our results to the experiments we need a relation between $\langle N_0\rangle$ and the average total number of particles. We already derived the average number of particles in the excited states $\langle N_{\mathsf{ex}}(T)\rangle$ in Eq. (2.7). The critical temperature T_c is defined by $\langle N\rangle = \langle N_{\mathsf{ex}}(T_c)\rangle$, i.e., all particles are in excited states, such that the ground state becomes occupied upon lowering the temperature. With this criterion, we find the relation $\langle N_{\mathsf{ex}}(T)\rangle = \langle N\rangle (T/T_c)^2$, which enables us to write for the average number of photons in the condensate

$$\langle N_0\rangle := \langle N\rangle - \langle N_{\mathsf{ex}}(T)\rangle = \frac{x}{3(1-x)}\left(\frac{\pi}{\hbar\beta\omega}\right)^2. \tag{3.5}$$

As expected, $\langle N_0\rangle \geq 0$ since the fraction x obeys $0 \leq x < 1$. With the expressions we derived in this section we are fully equiped to quantify number fluctuations in the condensate. However, first we investigate the legitimacy of the Gaussian variational ansatz in the next section.

3.3 Condensate Diameter

Within the variational treatment we performed above, q_{min} is a measure for the radius of the condensate. For a small number of particles, the wave function of the condensate approaches a Gaussian. We may define the diameter of the condensate as the full width at half maximum of the condensate density, which yields in this case $d_{\mathsf{gauss}} = 2q_{\mathsf{min}}\sqrt{\ln(2)}$. However, for a large number of condensate particles interactions between the particles become more important. The limiting case in which the interactions between the particles become much more important than the kinetic energy of the individual particles is called the Thomas-Fermi limit [24, 36]. In this case we expect a different density profile for the condensate. In fact, we can solve for this density profile by neglecting the kinetic term in Eq. (3.1) and minimizing with respect to the field $\phi_0^*(\mathbf{x})$. This yields for the condensate density

$$|\phi_0(\mathbf{x})|^2 = \left(\frac{\mu - m\omega^2|\mathbf{x}|^2/2}{g}\right)\theta(\mu - m\omega^2|\mathbf{x}|^2/2), \tag{3.6}$$

where the Heaviside function θ is introduced to make sure that the condensate density remains positive for all $\mathbf{x}$. We use this expression to find the relation between the number of particles in the condensate N_0 and the Thomas-Fermi radius of the photon condensate in two dimensions

$$N_0 = 2\pi\int_0^{R_{\mathsf{TF}}} r\left(\frac{\mu - m\omega^2 r^2/2}{g}\right)\mathrm{d}r = \frac{\pi}{4}m\omega^2 R_{\mathsf{TF}}^4, \tag{3.7}$$

such that $R_{\mathsf{TF}} = (4gN_0/\pi m\omega^2)^{1/4}$. Again we define the diameter of the condensate to be the full width at half maximum of the condensate density, which yields in this case $d_{\mathsf{TF}} = \sqrt{2}R_{\mathsf{TF}}$.

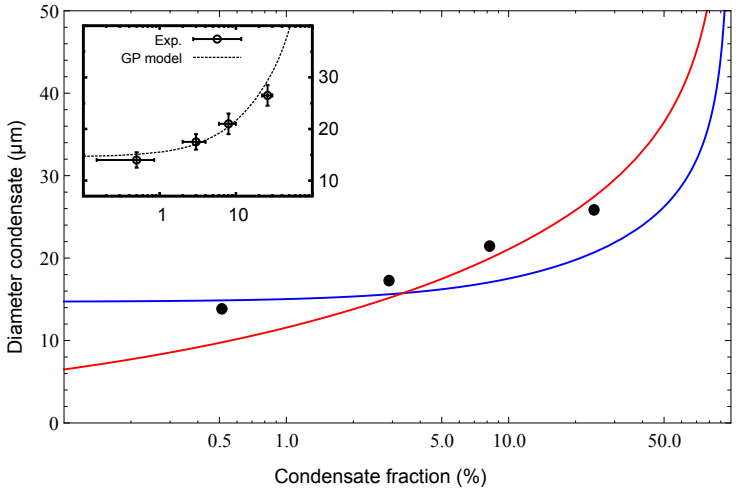

Figure 3.1: Plot of the diameter of the condensate in μm on a logarithmic scale of the condensate percentage. The included data points were kindly provided by J. Klaers and the inset is from Ref. [9]. The Gaussian diameter (blue) yields better results for smaller condensate fractions, whereas the Thomas-Fermi diameter (red) is better for larger condensate fractions. However, the qualitative behavior is similar. The inset shows the numerical solution of the Gross-Pitaevskii equation discussed in 2.6, which shows similar behavior.

We compare both expressions for the condensate diameter in Fig. 3.1, in which we included experimental data points for a condensate of photons, which were already discussed in Section 2.6. As expected, we observe that the Gaussian diameter works best for small condensate fractions and the Thomas-Fermi diameter for higher condensate fractions. However, the qualitative behavior of both approaches is the same for large condensate fractions. This is also known from condensates of dilute atomic gases [37]. This observation justifies the further use of the results we obtained within the Gaussian approximation in the previous section.

In the next section we briefly discuss how Schmitt *et al.* performed measurements on number fluctuations in a condensate of photons [10].

3.4 Measuring Number Fluctuations

The experimental setup used to detect the intensity correlations of condensed photons is displayed in Fig. 3.2. The first part of the setup is again the dye-filled optical microcavity pumped by an external laser beam as described in Chapter 1. What is new is that the light which leaks through the mirrors is guided through a mode filter. By selecting the photons on having zero transverse momentum, this apparatus makes sure that only condensed photons proceed to the next stage of the experiment. Subsequently, one can perform a Hanbury-Brown-Twiss experiment with the mode-filtered photons. In this experiment, the photon beam is split up into two beams by a beamsplitter. These two beams fall

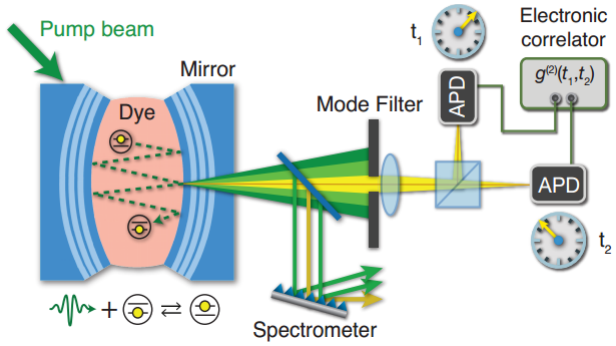

Figure 3.2: Experimental setup used to measure intensity correlations of condensed photons. Photons leaking through the mirrors of the microcavity are selected on having zero transverse momentum and then led through a Hanbury-Brown-Twiss experiment. The avalanche photodiodes (APD) have single photon sensitivity. Image taken from Ref. [10].

onto photo-diodes with a single-photon sensitivity and then an electronic correlator is used to make time histograms of the detection of single photons [10]. Using this setup, time correlations of the condensate population are determined in the form of the second-order correlation function, which is defined as

$$g^{(2)}(t_1, t_2) := \frac{\langle N_0(t_1) N_0(t_2)\rangle}{\langle N_0(t_1)\rangle\langle N_0(t_2)\rangle}, \tag{3.8}$$

where $\langle N_0(t)\rangle$ is the average number of photons in the condensate at time t. In fact, measurements indicate that the avarage number of photons in the condensate is independent of time. Additionally, one deduces from typical experimental results that the second-order correlations are only a function of the time delay τ in the arrival of two beams of photons on the detectors $\tau := t_2 - t_1$ [10]. It is therefore more interesting to consider the time-average second-order correlation function

$$g^{(2)}(\tau) := \langle g^{(2)}(t_1, t_2)\rangle_{t_2 - t_1 = \tau} = \frac{\langle N_0(0) N_0(\tau)\rangle}{\langle N_0(0)\rangle\langle N_0(\tau)\rangle}, \tag{3.9}$$

which can readily be measured in experiments. Photon bunching, i.e., $g^{(2)}(\tau) > 1$ is observed for small time delays in these experiments, as is expected when one performs a Hanbury-Brown-Twiss experiment with bosons. In fact, it is the zero-time delay autocorrelation function, given by

$$g^{(2)}(0) := \lim_{\tau \to 0} g^{(2)}(\tau) = \frac{\langle N_0^2\rangle}{\langle N_0\rangle^2} \tag{3.10}$$

which is most often used to quantify number fluctuations. Indeed, one can express the standard deviation of the number of photons in the condensate $\langle \delta N_0\rangle$ in terms of the zero-time delay autocorrelation function: $\langle \delta N_0\rangle = (g^{(2)}(0) - 1)^{1/2}\langle N_0\rangle$. Hence, if we know $g^{(2)}(0)$, we know how the number of particles in the condensate fluctuates. In general, $g^{(2)}(0) = 2$ for a single-mode thermal state and $g^{(2)}(0) = 1$ for a coherent state [21].

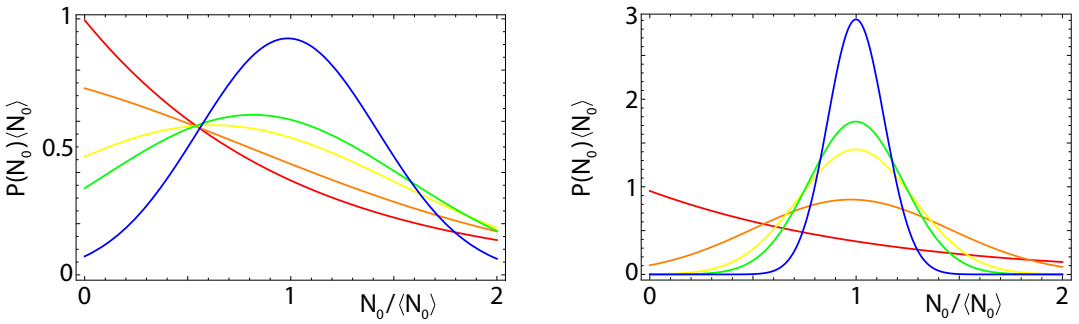

(a) $\tilde{g} = 5 \cdot 10^{-7}$ **(b)** $\tilde{g} = 5 \cdot 10^{-6}$

Figure 3.3: Typical plots of the probability distribution for the photons in the condensate for a fixed interaction strength and different condensate fractions $x_{\text{red}} = 0.04$, $x_{\text{orange}} = 0.28$, $x_{\text{yellow}} = 0.40$, $x_{\text{green}} = 0.45$ and $x_{\text{blue}} = 0.58$. We used a temperature of $T = 300$ K and a typical experimental value for the trapping frequency: $\omega = 8\pi \cdot 10^{10}$ Hz.

In the next section we self-consistently solve for the probability distribution for the number of photons in the condensate. With the probability distribution, we are able to calculate the zero-time delay autocorrelation function and compare it to the experimental results.

3.5 Comparison with Experiment

With the theory presented in Section 3.2 we are able to find the probability distribution in a self-consistent manner. The procedure is as follows. Given an interaction strength $\tilde{g}$, we use the normalized probability distribution in Eq. (3.4) to calculate the chemical potential as a function of $\langle N_0 \rangle$, i.e., $\mu = \mu(\langle N_0 \rangle)$. Given a condensate fraction x, we then use Eq. (3.5) to calculate $\langle N_0 \rangle$ and the corresponding μ. Finally, we use the obtained chemical potential to plot the probability distribution at fixed x and $\tilde{g}$. Typical plots of the probability distribution for different condensate fractions are displayed in Fig. 3.3. Clearly, we have exponential behavior due to a Poissonian process for small condensate fractions and Gaussian behavior for larger condensate fractions. Physically, this shows that the effect of repulsive interactions is to reduce number fluctuations, as the interactions give fluctuations an energy penalty. Increasing the interaction strength yields Gaussian behavior for even smaller condensate fractions. These Gaussians are also more strongly peaked around $\langle N_0 \rangle$ for higher interaction strengths, which is expected since stronger interactions between the bosons leads to the supression of fluctuations.

We can compare our theoretical curves from Fig. 3.3 for the probability distribution directly to experimental results obtained by Schmitt *et al.* These results are obtained with a similar setup to the one in Fig. 3.2. If one simply lets the mode-filtered photon beam fall onto a photomultiplier tube (instead of performing a Hanbury-Brown-Twiss experiment), the time evolution of the number of photons in the condensate can be measured. Typical measurements are displayed in Fig. 3.4a. The probability

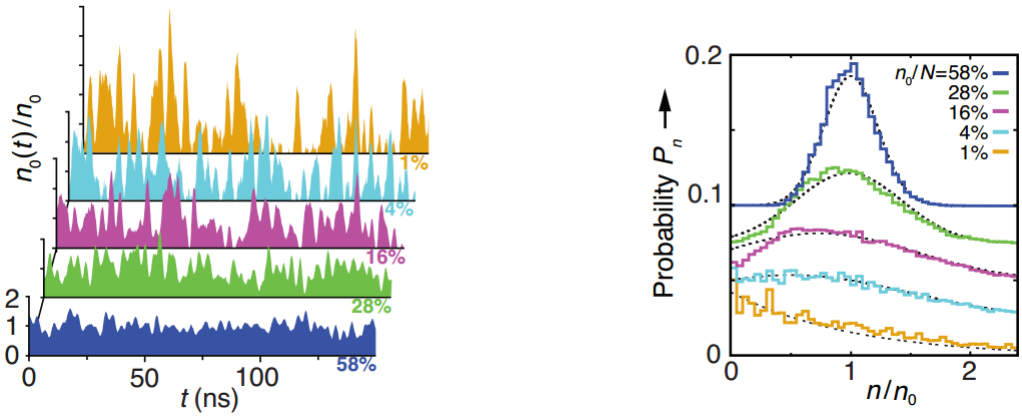

(a) Temporal occupation condensate mode

(b) Probability distribution condensate photon number

Figure 3.4: Fig. (a) shows the number of photons in the condensate mode as a function of time, normalized to the time-averaged number of photons in the condensate. The different curves correspond to different condensate fractions, ranging from 1% (orange) to 58% (dark blue). From this data, the probability distribution for the number of photons in the condensate can be calculated, as is displayed in Fig. (b) for the different condensate fractions. Images taken from Ref. [10].

distribution for the number of photons in the condensate $P(N_0)$ can be determined from these experiments. It is displayed for different condensate fractions in Fig. 3.4b. These experimental curves for the probability distribution should be compared to our theoretical curves in Fig. 3.3. We observe good agreement. In fact, we can exactly reproduce the experimental results for every condensate fraction by simply using the dimensionless interaction strength $\tilde{g}$ as a fitting parameter.

Next, we obtain the second moment $\langle N_0^2 \rangle$ from the probability distribution $P(N_0)$ in the same self-consistent manner. This gives us all the information needed to quantify the number fluctuations of the condensate in terms of the zero-time delay autocorrelation function $g^{(2)}(0)$. A plot of $g^{(2)}(0)$ against the condensate fraction is displayed in Fig. 3.5 for different interaction strengths $\tilde{g}$. Theoretically, we know that for thermal photons $g^{(2)}(0) = 2$ [21], which is exactly what we observe in our plots for the corresponding case $x = 0$. If all photons in the cavity are part of the condensate, i.e., for a condensate fraction of unity, we have the coherent state result $g^{(2)}(0) = 1$. The interpretation of the behavior in between these limits is as follows. Suppose we fix the condensate fraction x. At small interactions the quartic term in the energy in Eq. (3.1) is small and the minima of the energy are small and broad, yielding large number fluctuations. If we increase the interaction, the minima become deeper and more narrow, effectively reducing the fluctuations. The same reasoning holds for a fixed interaction strength and increasing condensate fractions.

In Fig. 3.5 we also plotted the experimental data points of Ref. [18]. Note that experimentalists stress that the experimental data points for small condensate fractions are unreliable due to systematic measurement errors. Roughly what happens is that the condensate spot, as displayed in Fig. 2.4b, becomes

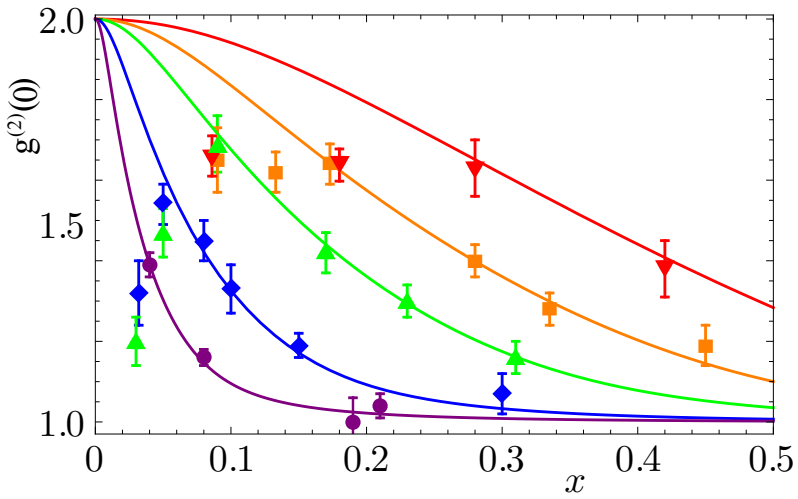

Figure 3.5: Plot of the zero-time delay autocorrelation function $g^{(2)}(0)$ against the condensate fraction x for $\omega = 8\pi \cdot 10^{10}$ Hz and $T = 300$ K. The different curves correspond to different interaction strengths: $\tilde{g}_{\text{red}} = 5 \cdot 10^{-7}$, $\tilde{g}_{\text{orange}} = 2 \cdot 10^{-6}$, $\tilde{g}_{\text{green}} = 5 \cdot 10^{-6}$, $\tilde{g}_{\text{blue}} = 3 \cdot 10^{-5}$, $\tilde{g}_{\text{purple}} = 2 \cdot 10^{-4}$. All curves are compared to the included experimental points from Schmitt *et al.* [18]. The experimental results for small condensate fraction x are unreliable due to systematic measurement errors. Indeed, theoretically we have $\lim_{x\to 0} g^{(2)}(0) = 2$.

smaller for decreasing condensate fractions. This makes it more difficult to filter out the noncondensed photons from the condensed photons.

We are able to reproduce all data sets in Fig. 3.5 by tuning the interaction parameter $\tilde{g}$. Unfortunately, only one experimental value for $\tilde{g}$ is known. By measuring the size of the condensate for different condensate fractions, it was experimentally found that $\tilde{g} = (7 \pm 3) \cdot 10^{-4}$ [9], which only differs a factor of two with our result for the purple curve $g_{\text{purple}} = 2 \cdot 10^{-4}$. However, we note that the trapping potential, concentration of dye molecules and effective photon mass were somewhat different for the purple data points and the measurement of the interaction strength. We expect the interaction strength to vary smoothly with variations in the experimental parameters. Hence, the agreement is remarkable and points to the important role of interactions on number fluctuations in these experiments.

Furthermore, we note that the data points in Fig. 3.5 were obtained for different dye molecule densities n_{mol} and detunings $\delta := \hbar(\omega_{\text{cutoff}} - \omega_0)$, which is the difference between the low-frequency cavity cutoff and the dye specific zero-phonon line frequency, which we introduced in Fig. 2.3. The used values for δ and n_{mol} for the curves in Fig. 3.5 are included in Fig. 3.6. Within our theory, the dependence of number fluctuations on these parameters can be incorporated via their influence on the interactions. Therefore, it would be useful to perform systematic measurements of $\tilde{g}$ for different detunings and molecule concentrations, as is also proposed in Ref. [38]. With this information, we would be able to directly compare all experimental results with our theoretical predictions for the number fluctuations.

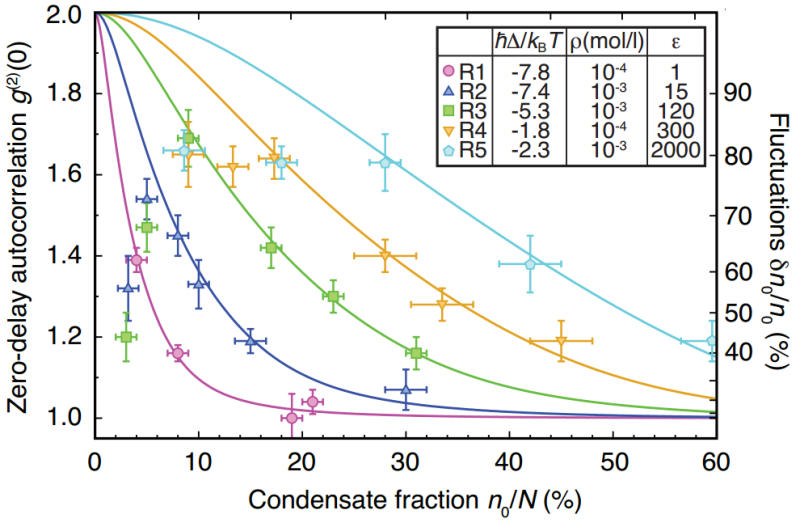

Figure 3.6: Fits to the experimental results for $g^{(2)}(0)$ based on a different model as explained in Ref. [20]. The fitting parameter $\bar{\epsilon} := M_{\text{eff}}/M$ quantifies the "effective reservoir size" of the heat bath of molecules, M_{eff}, to its real value M. The figure is a revised version of an image in Ref. [10].

Before we continue with discussing possible interaction mechanisms for the photon-photon interaction, we first discuss a different explanation for the experimental results displayed in Fig. 3.5.

3.6 A Different Explanation?

In Ref. [20] Klaers *et al.* consider a different model to explain the experimental results of Fig. 3.5. In this alternative model no photon-photon interaction is assumed. Still, the authors are able to obtain similar results to ours for $g^{(2)}(0)$, by using a single fitting parameter. These fits are displayed in Fig. 3.6. On the other hand, the theory we presented in this chapter is entirely based on photon-photon interactions, suggesting that one of the theories might be less appropriate for the system at hand. Therefore, we briefly discuss this alternative theory and try to indicate where it deviates from our own theory.

Klaers *et al.* consider a master equation for the probability $p_n(t)$ to find n photons in the condensate. The molecules are modeled as two-level systems and the system has a corresponding absorption coefficient A and a rate E of spontaneous and stimulated emission. Additionally, the sum of the number of photons in the lowest cavity mode and the number of excited molecules, defined as X, is assumed

to be constant. The authors argue that the master equation is given by

$$\begin{aligned}\dot{p}_n = &En(X-n+1)p_{n-1} - E(n+1)(X-n)p_n \\ &+ A(n+1)(M-X+n+1)p_{n+1} - An(M-X+n)p_n,\end{aligned} \tag{3.11}$$

where M is the total number of molecules, $X-n$ is the number of electronically excited molecules and $M-X+n$ is the number of ground-state molecules. Note that by writing down this master equation, the molecules are considered to be in a single mode, i.e., without any center-of-mass translational degrees of freedom. As there are many momentum modes available to the dye molecules at room temperature, this might not be an appropriate statistical description.

By assuming that the probability $p_n(t)$ becomes stationary for large times, one finds a solution to the master equation Eq. (3.11) by recursive substitution

$$\frac{p_n(t\to\infty)}{p_0} = \frac{(M-X)!X!}{(M-X+n)!(X-n)!}\exp\left(-n\beta\delta\right), \tag{3.12}$$

where $\delta := \hbar(\omega_{\text{cutoff}} - \omega_0)$ is the dye-cavity detuning we introduced earlier. Note that if one uses this probability distribution to calculate the average number of photons in the condensate $\langle n\rangle$, one does not find a Bose-Einstein distribution. In Appendix A.1 we treat the system grand-canonically and write down a master equation similar to Eq. (3.11). We show that in this treatment, we do obtain a Bose-Einstein distribution for the average number of photons in the condensate.

Furthermore, by using the probability distribution Eq. (3.11), the authors do a similar calculation to ours and obtain the curves in Fig. 3.6. The fitting parameter $\bar{\epsilon}$ is used to quantify the, what the authors call, "effective reservoir size" M_{eff}, by $\bar{\epsilon} = M_{\text{eff}}/M$. Notice that this effective reservoir size M_{eff} is varied up to two thousand times its 'real value' M to reproduce the experimental results. Additionally, the experimental data is interpreted by the authors as signaling a transition from the canonical to the grand-canonical regime. However, the absolute value of the effective molecular heat bath varies from 10^9 to 10^{10} dye molecules, which usually is sufficiently large for there to be no difference in the choice of ensemble. We believe this behavior is a result of the assumption that the molecules do not have center-of-mass translational degrees of freedom.

Summarizing, we have tried to indicate where the alternative model by Klaers *et al.* deviates from our own model, which is based on the assumption of a photon-photon interaction. In the next sections, we focus on the possible microscopic origin of this interaction.

3.7 Possible Photon-Photon Interactions

The question remains what microscopic mechanism causes a photon-photon interaction that depends on both n_{mol} and the detuning δ. In fact, we conclude from the experimental data in Ref. [18] that

the interaction behaves counter-intuitively: it decreases both for an increasing molecule density and for a decreasing detuning. Three different mechanisms are expected to play a role[1] [38]:

1) Thermal lensing;

2) Kerr nonlinearities;

3) Dye-mediated photon-photon scattering.

The first mechanism is due to a temperature-dependence of the index of refraction. We set up a model for this in the following subsection and use it to estimate the resulting dimensionless interaction strength. The other two mechanisms are due to nonlinearities, i.e., the index of refraction is intensity dependent due to the properties of the solvent molecules (the Kerr effect), or due to photon-photon scattering mediated by the dye molecules. The former effect has been investigated in Refs. [38, 39] and turns out to be negligible. We therefore consider the latter effect in subsection 3.7.2 in the form of a box diagram and use it to calculate the dimensionless interaction strength resulting from this effect.

3.7.1 Thermal Lensing

Thermal lensing is the phenomenon that the index of refraction n depends on the temperature of the medium. In the experiment of interest to us, nonradiative decay of the dye molecules, local fluctuations in the photon number and the external pumping with a laser lead to temperature fluctuations around the average temperature T_0. For a homogeneous temperature distribution this implies, to lowest order, that $n(T) = n(T_0) + \epsilon(T - T_0)$. As the photon energy Eq. (2.3) depends on the index of refraction via the speed of light in the medium, these temperature fluctuations couple to the photons, as we show explicitly below.

We model this mechanism by assuming that the temperature fluctuations behave diffusively. Thus, we consider the following action in imaginary time for the complex-valued photon field $\phi(\mathbf{r}, \tau)$ and the real-valued temperature fluctuation field $\delta T(\mathbf{r}, \tau)$

$$S[\phi, \phi^*, \delta T] = \int \mathrm{d}\mathbf{r} \int \mathrm{d}\tau \Bigg[\phi^*(\mathbf{r}, \tau) \left(\hbar \frac{\partial}{\partial \tau} - \frac{\hbar^2 \nabla_{\mathbf{x}}^2}{2m} - \frac{mc^2}{n^2} + \frac{1}{2} m\omega^2 |\mathbf{x}|^2 - \mu \right) \phi(\mathbf{r}, \tau) + \frac{\delta T(\mathbf{r}, \tau)}{2T_0} \left(c_p + \frac{\kappa \nabla_{\mathbf{r}}^2}{i \partial_\tau} \right) \delta T(\mathbf{r}, \tau) \Bigg], \tag{3.13}$$

where $\mathbf{r} = (x, y, z)$ is a three-dimensional vector, $\mathbf{x} = (x, y)$ the two-dimensional transverse vector, $\nabla_{\mathbf{x}}^2$ denotes that we only consider motion in the transversal direction, c_p is the heat capacity of

[1] Private correspondence with J. Klaers and M. Weitz.

the solution and κ the thermal conductivity of the solution. The part which is quadratic in the temperature fluctuations is constructed such that it has the correct diffusive pole and diffusion propagator.

To include thermal lensing, we now write for the index of refraction $n(T) = n(T_0) + \epsilon\delta T(\mathbf{r},\tau)$, whilst keeping k_z fixed. Substituting this into the action and expanding for small temperature fluctuations, we obtain

$$S[\phi,\phi^*,\delta T] = \int \mathrm{d}\mathbf{r} \int \mathrm{d}\tau \Bigg[\phi^*(\mathbf{r},\tau) \left(\hbar\frac{\partial}{\partial\tau} - \frac{\hbar^2\nabla^2_{\mathbf{x}}}{2m} + \frac{1}{2}m\omega^2|\mathbf{x}|^2 - \mu + \frac{mc^2\epsilon}{n^2(T_0)}\delta T(\mathbf{r},\tau) \right) \phi(\mathbf{r},\tau) + \frac{\delta T(\mathbf{r},\tau)}{2T_0} \left(c_p + \frac{\kappa\nabla^2_{\mathbf{r}}}{i\partial_\tau} \right) \delta T(\mathbf{r},\tau) \Bigg], \tag{3.14}$$

where we removed a constant offset in the energy by redefining the chemical potential μ with respect to this ground-state energy. Furthermore we note that the field $\phi(\mathbf{r},\tau)$ has an equation of motion in the longitudinal direction which decouples, such that we may write $\phi(\mathbf{r},\tau) = \phi_{\mathsf{long}}(z)\phi_{\mathsf{trans}}(\mathbf{x},\tau)$, with $\phi_{\mathsf{long}}(z)$ the photon field in the longitudinal direction and $\phi_{\mathsf{trans}}(\mathbf{x},\tau)$ the photon field in the transverse direction. Similar to our derivation of the effective photon dispersion relation Eq. (2.3) in Chapter 2, we assume metallic boundary conditions and demand that the longitudinal part of the photon field is a standing wave. We obtain the normalized longitudinal solution

$$\phi_{\mathsf{long}}(z) = \sqrt{\frac{2}{D_0}} \sin\left(\frac{q\pi z}{D_0}\right), \tag{3.15}$$

with D_0 distance between the centers of the cavity mirrors and $q \in \mathbb{N}_{>0}$. Subsituting this longitudinal solution into the action Eq. (3.14) and using the fact that it is normalized, we find

$$S[\phi,\phi^*,\delta T] = \int \mathrm{d}\mathbf{x} \int \mathrm{d}\tau\ \phi^*_{\mathsf{trans}}(\mathbf{x},\tau) \left(\hbar\frac{\partial}{\partial\tau} - \frac{\hbar^2\nabla^2_{\mathbf{x}}}{2m} + \frac{1}{2}m\omega^2|\mathbf{x}|^2 - \mu \right) \phi_{\mathsf{trans}}(\mathbf{x},\tau) + \int \mathrm{d}\mathbf{r} \int \mathrm{d}\tau \left[\frac{\delta T(\mathbf{r},\tau)}{2T_0} \left(c_p + \frac{\kappa\nabla^2_{\mathbf{r}}}{i\partial_\tau} \right) \delta T(\mathbf{r},\tau) + \frac{mc^2\epsilon}{n^2(T_0)}\delta T(\mathbf{r},\tau)\phi^*(\mathbf{r},\tau)\phi(\mathbf{r},\tau) \right]. \tag{3.16}$$

Note that the last term in the expression above represents a coupling between the photons and the temperature fluctuations in the form of an interaction vertex. Now we would like to find an effective action for the photon field by integrating out these temperature fluctuations. By going to Fourier space we show in Appendix A.2 that the effective action reads

$$S^{\mathsf{eff}}[a,a^*] = \sum_{\mathbf{k},n} a^*_{\mathbf{k},n}(-\hbar G^{-1}_\gamma(\mathbf{k},i\omega_n))a_{\mathbf{k},n} - \frac{1}{\hbar^2\beta V}\left(\frac{mc^2\epsilon}{2n^2(T_0)}\right)^2 \sum_{\substack{\mathbf{k},\mathbf{p},\mathbf{k}' \\ n,m,n'}} G_T(\mathbf{p},\omega_m) a^*_{\mathbf{k}+\mathbf{p},n+m} a_{\mathbf{k},n} a^*_{\mathbf{k}',n'} a_{\mathbf{k}'+\mathbf{p},n'+m}, \tag{3.17}$$

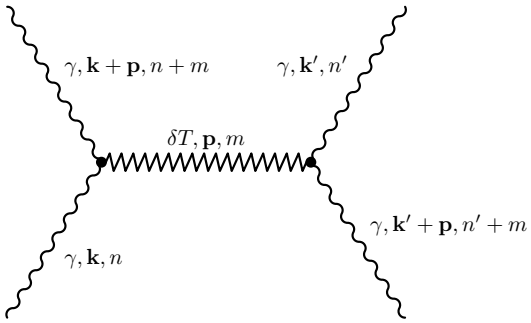

Figure 3.7: Feynman diagram for the photon-photon interaction due to exchange of temperature fluctuations δT (zigzag propagator). The photons γ are indicated by a wiggly propagator.

where we omitted an uninteresting term and we defined the inverse photon propagator $-\hbar G_\gamma^{-1}(\mathbf{k}, i\omega_n) := -i\hbar\omega_n + \epsilon_\gamma(\mathbf{k}) - \mu$. The last term in the effective action gives us the effective photon-photon interaction due to the coupling of the photons to the temperature fluctuations. It is graphically depicted as a Feynman diagram in Fig. 3.7. We read off the associated photon-photon four-point vertex

$$\Gamma^{(4)}_{\mathsf{3D}}(\mathbf{p}, \omega_m) = -\frac{2}{\hbar} G_T(\mathbf{p}, \omega_m) \left(\frac{mc^2\epsilon}{2n^2(T_0)} \right)^2 . \tag{3.18}$$

Note that we extracted a factor of $(2\hbar\beta V)^{-1}$, as is the convention for a four-point vertex in the imaginary time formalism [36]. By dimensional analysis, we note that $[\Gamma^{(4)}_{\mathsf{3D}}] = \mathrm{J{\cdot}m^3}$. Hence, as the photon gas is confined to two dimensions we must scale this quantity to

$$\Gamma^{(4)}_{\mathsf{2D}}(\mathbf{p}, \omega_m) = \left(\int_0^{D_0} |\phi_{\mathsf{long}}(z)|^4 \, \mathrm{d}z \right) \Gamma^{(4)}_{\mathsf{3D}}(\mathbf{p}, \omega_m) = \frac{2\Gamma^{(4)}_{\mathsf{3D}}(\mathbf{p}, \omega_m)}{3D_0}, \tag{3.19}$$

where we used the solution for the longitudinal photon field Eq. (3.15). Note that the integral does not depend on the value for q. Now we do have $[\Gamma^{(4)}_{\mathsf{2D}}] = \mathrm{J{\cdot}m^2}$. With this expression for the four-point vertex, we calculate the effective dimensionless coupling constant $\tilde{g}$ of the photons in the condensate due to thermal lensing. Taking the photons in the condensate, i.e., with Matsubara frequency zero and only a nonzero momentum of k_z in the z-direction, we obtain[2]

$$\tilde{g} = \frac{m\Gamma^{(4)}_{\mathsf{2D}}(\mathbf{0}, 0)}{\hbar^2} = \frac{m^3c^4\epsilon^2 T_0}{3D_0\hbar^2 n^4(T_0) c_p}. \tag{3.20}$$

Note that this expression has neither an explicit dependence on the detuning δ, nor on the concentration of dye molecules n_{mol}, as it is fully determined by the properties of the solvent. Both the temperature dependence of the single-photon energy and the heat capacity might depend on the number of dissolved

[2]Note that as all condensate photons have momentum $\mathbf{k}_+ = (0, 0, k_z)$, conservation of momentum in the Feynman diagram Fig. 3.7 implies that the three-dimensional temperature momentum must be identical to zero, i.e., $\mathbf{p} = 0$.

dye molecules, but as the experiments by Schmitt *et al.* are performed for small concentrations of dissolved Rhodamine 6G, we expect at least this latter effect to be small. Typical numerical values for the constants in Eq. (3.20) for liquid methanol with 10^{-3} mol·L^{-1} Rhodamine 6G dissolved at room temperature are

- $n = 1.34$;
- $\epsilon = -5 \cdot 10^{-4}$ K^{-1} [40];
- $c_p = \tilde{c}_p / V_m$ with $\tilde{c}_p = 79.5$ J·mol^{-1}·K^{-1} and $V_m = 40.0 \cdot 10^{-6}$ m^3·mol^{-1} [41].

Furthermore we use the typical values $m = 6.7 \cdot 10^{-36}$ kg, $D_0 = 1.46 \cdot 10^{-6}$ m [9], yielding an estimate for the interaction strength of $\tilde{g} \sim 10^{-9}$. This is several orders of magnitude below the only experimental result $\tilde{g} \sim 10^{-4}$. Together with the fact that Eq. (3.20) does not have the correct behavior as a function of δ and n_{mol}, this suggests that thermal lensing is not the dominant interaction effect.

Thus, we need to consider another microscopic mechanism for the photon-photon interaction. One possible candidate is a nonlinearity due to the Kerr effect [38]. This effect is of an optoelectrical nature and is caused by a change of the refractive index in a medium due to an applied electric field. In the experiment at hand, the electric field is provided by the photons in the cavity. However, this effect does not seem to depend on the dye molecules explicitly. Furthermore it was estimated in Ref. [38] to be too small.

As described before, photon-photon scattering mediated by dye molecules is another possible candidate. Intuitively we expect that this mechanisms at least depends on the concentration of dye molecules. We estimate its size in the next subsection.

3.7.2 Dye-Mediated Photon-Photon Scattering

We now neglect the temperature depence of the index of refraction and focus on dye-mediated photon-photon scattering. Additionally, we neglect the harmonic trapping potential for the photons, since this is not important for the coupling between the photons and the molecules. We therefore consider the following Euclidean action which includes the interactions between the photons and the molecules [42]

$$\begin{aligned} S = &\sum_{\mathbf{k},n} a^*_{\mathbf{k},n}(-i\hbar\omega_n + \epsilon_\gamma(\mathbf{k}) - \mu) a_{\mathbf{k},n} + \sum_{\mathbf{p},\rho,n} b^*_{\mathbf{p},\rho,n}(-i\hbar\omega_n + \epsilon(\mathbf{p}) - \mu_\rho + K_\rho) b_{\mathbf{p},\rho,n} \\ &+ \frac{g_{\text{mol}}}{\sqrt{\hbar\beta V}} \sum_{\mathbf{k},\mathbf{p},n,n'} \left(a_{\mathbf{k},n} b_{\mathbf{p},\downarrow,n'} b^*_{\mathbf{p}+\mathbf{k},\uparrow,n+n'} + a^*_{\mathbf{k},n} b_{\mathbf{p}+\mathbf{k},\uparrow,n+n'} b^*_{\mathbf{p},\downarrow,n'} \right), \end{aligned} \tag{3.21}$$

with $\rho \in \{\uparrow, \downarrow\}$, V is the three-dimensional volume of the system, g_{mol} is the coupling constant between the photons and the molecules, $\epsilon(\mathbf{p}) = \hbar^2 |\mathbf{p}|^2 / 2M$ is the dispersion relation for the molecules

with mass M and $\epsilon_\gamma(\mathbf{k}) = \hbar c\sqrt{k_x^2 + k_y^2 + k_z^2}$ the dispersion relation for the photons[3] , in which k_z is the fixed longitudinal momentum and c the speed of light in the medium. We use the convention that a sum over $\mathbf{p}$ is three-dimensional, whereas a sum over $\mathbf{k}$ is a two-dimensional sum over a three-dimensional vector with a fixed z-component. Furthermore, we introduced the photon field amplitude $a_{\mathbf{k},n}$ and molecule field amplitude $b_{\mathbf{p},\rho,n}$. The photon fields are bosonic and we model the molecules as fermions, although this is not important since in the end we always consider the classical limit for the dye molecules. Additionally, we model the molecules as a two-level system consisting of an excited state ($\uparrow$) and ground state ($\downarrow$), with corresponding chemical potentials $\mu_\uparrow$ and $\mu_\downarrow$, and associated energies $K_\uparrow = \Delta$ and $K_\downarrow = 0$. Finally, the last two terms describe the absorption and emission of a photon by a dye molecule.

From the action Eq. (3.21) we read off the propagators of the noninteracting theory in Fourier space

$$\begin{cases} G_\gamma(\mathbf{k}, i\omega_n) = \dfrac{-\hbar}{-i\hbar\omega_n + \epsilon_\gamma(\mathbf{k}) - \mu}, \\ G_\rho(\mathbf{p}, i\omega_n) = \dfrac{-\hbar}{-i\hbar\omega_n + \epsilon(\mathbf{p}) - \mu_\rho + K_\rho}, \end{cases} \tag{3.22}$$

with ω_n denote the appropriate Matsubara frequencies. In Appendix A.3 we derive an effective action for the photons by integrating out the molecular fields in Eq. (3.21). It reads

$$\begin{aligned} S^{\text{eff}}[a^*, a] = &\sum_{\mathbf{k},n} a^*_{\mathbf{k},n}\Big(- i\hbar\omega_n + \epsilon_\gamma(\mathbf{k}) - \mu + \hbar\Sigma(\mathbf{k}, i\omega_n)\Big) a_{\mathbf{k},n} \\ &+ \frac{1}{2\hbar\beta V} \sum_{\substack{\mathbf{k},\mathbf{k}',\mathbf{k}'' \\ n,n',n''}} \Gamma^{(4)}(\mathbf{k}, \mathbf{k}', \mathbf{k}'', i\omega_n, i\omega_{n'}, i\omega_{n''}) a^*_{\mathbf{k},n} a_{\mathbf{k}',n'} a^*_{\mathbf{k}'',n''} a_{\mathbf{k}-\mathbf{k}'+\mathbf{k}'',n-n'+n''}, \end{aligned} \tag{3.23}$$

where we defined the self-energy as

$$\hbar\Sigma(\mathbf{k}, i\omega_n) := \frac{g^2_{\text{mol}}}{\hbar^2\beta V} \sum_{\mathbf{p},m} G_\downarrow(\mathbf{p}, i\omega_m) G_\uparrow(\mathbf{p}+\mathbf{k}, i(\omega_n + \omega_m)), \tag{3.24}$$

and the photon-photon interaction vertex is defined as

$$\begin{aligned} &\Gamma^{(4)}(\mathbf{k}, \mathbf{k}', \mathbf{k}'', i\omega_n, i\omega_{n'}, i\omega_{n''}) := \\ &\quad - \frac{g^4_{\text{mol}}}{\hbar^4\beta V} \sum_{\mathbf{p},m} G_\uparrow(\mathbf{p}+\mathbf{k}, i(\omega_m + \omega_n)) G_\downarrow(\mathbf{p}, i\omega_m) G_\uparrow(\mathbf{p}+\mathbf{k}', i(\omega_m + \omega_{n'})) \\ &\qquad\qquad \times G_\downarrow(\mathbf{p}+\mathbf{k}'-\mathbf{k}'', i(\omega_m + \omega_{n'} - \omega_{n''})). \end{aligned} \tag{3.25}$$

Graphically, the photon self-energy and the photon-photon interaction vertex are depicted in Fig. 3.8. To make an estimate of the interaction strength resulting from the photon-photon interaction vertex

[3] Contrary to Chapter 2 we now use a subscript γ to distinguish between the dispersion relation of the photons and that of the molecules.

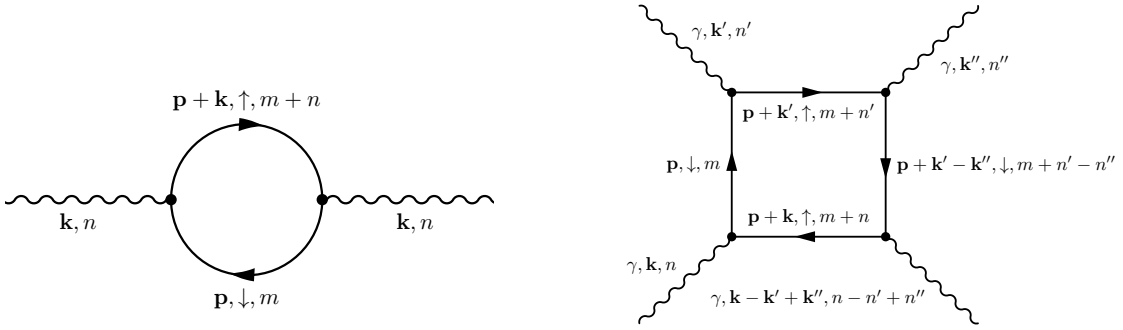

(a) Photon self-energy diagram, Eq. (3.24) **(b)** Photon-photon scattering diagram, Eq. (3.25)

Figure 3.8: Feynman diagrams for the photon self-energy and photon-photon interaction vertex. Wiggly lines indicate photon propagators. In both diagrams the molecule (straight line propagator) forms a closed loop of ground ($\downarrow$) and excited ($\uparrow$) states. Matsubara frequencies ω_m are denoted as m.

Eq. (3.25), we need numerical values for the coupling constant g_{mol} and for the energy difference Δ between the ground state and excited state of the dye molecules. It turns out that the interaction vertex actually diverges. This can be resolved by a rather intuitive solution: we assign a finite lifetime to the excited states of the molecules, quantified by the decay rate Γ. Similar to the procedure followed in Ref. [42] we use Fermi's golden rule to calculate the absorption spectrum of the dye as a function of the frequency ω. Subsequently, we can fit this to the experimental absorption spectrum of the dye and obtain the necessary constants.

By modelling the dye molecules as classical particles, i.e., obeying a Maxwell-Boltzmann distribution, we show in Appendix A.4 that the absorption cross section at equilibrium is given by

$$\sigma_{\mathsf{abs}}(\omega) = \frac{\sqrt{2\pi} g_{\mathsf{mol}}^2}{\hbar^2 \Gamma c} \exp\left(-\frac{(\hbar\omega - \Delta)^2}{2\hbar^2\Gamma^2}\right). \tag{3.26}$$

We compare this expression quantitatively to the experimental data for the fluorescent dye [43, 44]. The absorption spectrum for the dye is asymmetric and impossible to fully reproduce within this simple treatment. However, we can perform a fit to the line shape and obtain typical values such as

- $g_{\mathsf{mol}} = 4 \cdot 10^{-33}$ J·m$^{3/2}$;
- $\Gamma = 1.15 \cdot 10^{14}$ Hz;
- $\Delta = 3.8 \cdot 10^{-19}$ J.

The found value for Δ is very close to the value found in Ref. [42], where the dye molecules were also modeled as a two-level system, but without a finite lifetime for the excited state. However, the value for Γ seems to be rather large. In Section 2.3 we noted that the lifetime of the excited states in the dye molecules is of the order of nanoseconds. An estimate of the lifetime τ we have obtained now

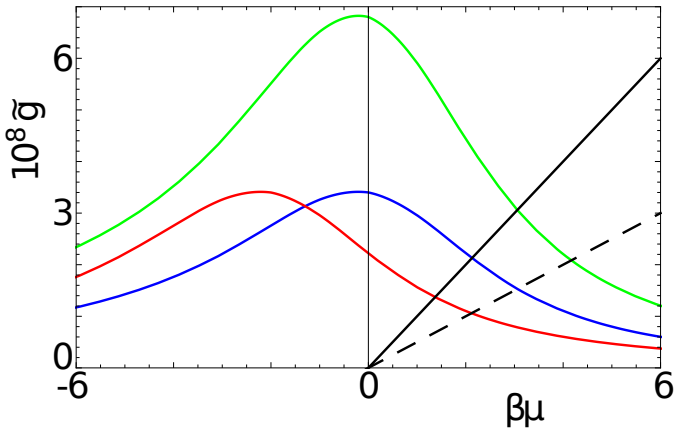

Figure 3.9: Dimensionless interaction parameter $\tilde{g}$ as a function of the chemical potential $\beta\mu$. We used $T = 300$ K, $\beta\hbar\Gamma = 2.9$, $D_0 = 1.46$ μm, $g_{\text{mol}} = 4.1 \cdot 10^{-33}$ J·m$^{3/2}$ (chosen such that we reproduce the photon self-energy) and $m = 6.7 \cdot 10^{-36}$ kg. The blue curve is for $n_{\text{mol}} = 9 \cdot 10^{23}$ m^{-3} and $\beta\delta = 4.9$. The green curve has twice the molecule density and the red curve has unchanged n_{mol} but $\beta\delta_{\text{red}} = 2.9$. As an illustration, the black curve has slope 10^{-8} and the dashed black curve $0.5 \cdot 10^{-8}$. The intersection of the black and blue curve yields the correct μ for the parameters of the blue curve. Doubling n_{mol} we can either find the intersection of the green curve and the black line, or the intersection of the blue curve with the dashed curve, which has half the slope. In the latter case we explicitly see $\tilde{g}$ decreasing.

is simply $\tau \sim 1/\Gamma$, which is significantly smaller than nanoseconds. This indicates that the two-level approximation might not be very good. Still, for now we continue with these results.

Subsequently, we evaluate the photon-photon interaction vertex Eq. (3.25) in Appendix A.5 for photons in the condensate, i.e., with Matsubara frequency zero and momentum $\mathbf{k}_+ = (0, 0, k_z)$. The resulting dimensionless interaction parameter is given by

$$\tilde{g}(\mu) = \frac{m g_{\text{mol}}^4 \beta n_{\text{mol}}}{\hbar^4 \Gamma^2 D_0} f(\beta\mu - \beta\delta), \tag{3.27}$$

with $f(\beta\mu - \beta\delta)$ is a smooth dimensionless function peaked around zero, which cannot be determined analytically. Although we have now found this expression for $\tilde{g}$, we still have to solve for $\tilde{g}(\mu)$ self-consistently with the Gross-Pitaevskii equation Eq. (2.9). Considering the center of the trap, i.e., $V^{\text{ex}} = 0$, this amounts to solving

$$\tilde{g}(\mu) = \frac{m\mu}{\hbar^2 n_{\text{ph}}} \tag{3.28}$$

for μ, with n_{ph} the photon density. Graphically, this means that we need to find the intersection of $\tilde{g}(\mu)$ and $(m/\hbar^2 n_{\text{ph}})\mu$. After finding the intersection value μ_{int}, this should be reinserted into Eq. (3.27) to yield the self-consistent dimensionless interaction strength $\tilde{g}(\mu_{\text{int}})$. Typical value for the densities are

- $n_{\text{ph}} \simeq 10^{12}$ m^{-2} [42];

- $n_{\mathsf{mol}} \simeq 9 \cdot 10^{23}$ m^{-3} [42],

yielding for the dimensionless interaction strength an estimate of $\tilde{g} \sim 10^{-8} - 10^{-7}$. This is still rather small compared to the experimental value of $\tilde{g} \sim 10^{-4}$. However, the magnitude of $\tilde{g}$ is rather uncertain due to the simplification of the rovibrational energy spectrum of the dye molecules to a two-level system. A thorough treatment in which all excited states in the rovibrational manifold have a different coupling strength to the photons might change the size of the interaction strength considerably. Interestingly, this box diagram does have the correct behavior as a function of δ and n_{mol}, as we discuss now.

If the magnitude of $\tilde{g}$ and the slope $m/\hbar^2 n_{\mathsf{ph}}$ are such that the intersection occurs on the right side of the peak in $\tilde{g}$, increasing the molecule density (and thus proportionally $\tilde{g}$) means that the point of intersection moves to the right. This implies that the strength of the interaction decreases. A graphical representation is given in Fig. 3.9. This is exactly the counter-intuitive behavior we are looking for. In order to relate the interaction strength $\tilde{g}$ to the detuning, we note that $\tilde{g}$ only depends on $\mu - \delta$. Therefore, by changing δ we shift the position of the maximum of $\tilde{g}$. Thus, if we alter δ such that $\tilde{g}$ moves to the left, the interaction strength decreases. In conclusion, this box diagram yields a possible mechanism for the counter-intuitive behavior of the interaction that we found by comparing our theory for photon condensate-number fluctuations to available experiments [18].

3.8 Conclusion

In this chapter we presented a general theory to calculate number flucutations in harmonically trapped Bose-Einstein condensates. The crucial ingredient was the introduction of a nonvanishing photon-photon interaction strength. Comparing our results with recent experiments on a condensate of light, we found good quantitative agreement. However, systematic measurements of the interaction strength are necessary to understand the true nature of the interaction. In the literature thermal lensing is expected to be the dominant interaction mechanism in the condensate of photons. However, we performed a microscopic calculation to estimate its size and found that it is in fact too small. As an alternative mechanism we proposed a nonlinearity in the form of dye-mediated photon-photon scattering. This mechanism appears to have the correct behavior as a function of the concentration of dye molecules, but was also found to be small. We argued that this might be due to the fact that we oversimplified the difficult dye molecules to a two-level system. Finally, we note that if the interaction is indeed a contact interaction at long wavelengths, then this would imply that the photon condensate is also a superfluid.

Chapter 4

Phase Diffusion in a Condensate of Light

In this chapter we study phase diffusion in a Bose-Einstein condensate of photons. After introducing the concept of phase diffusion in the introduction, we propose an interference experiment between the condensed photons and an external laser to measure phase diffusion in the photonic condensate. Since phase diffusion is governed by both quantum and thermal fluctuations of the number of condensed particles, we calculate average interference patterns for both cases seperately. We treat the quantum fluctuations by deriving and solving a Schrödinger-type equation for the phase. For the thermal fluctuations we derive a set of stochastic differential equations for the phase of the condensate and the number of particles in the condensate. For the at present experimentally most relevant situation where thermal fluctuations dominate, we conclude that representative results of individual measurements can be obtained from the stochastic equations.

The contents of this chapter have been submitted for publication in the Physical Review Letters as *"Phase diffusion in a Bose-Einstein condensate of light"*, A.-W. de Leeuw, E.C.I. van der Wurff, R.A. Duine and H.T.C. Stoof.

4.1 Introduction

Phase transitions are every-day phenomena that have many high-tech applications in daily life, such as for example the isotropic-nematic phase transition in LCD screens. Additionally, phase transitions are often encountered in fundamental research, such as in the description of superconductivity [45] and the electroweak and QCD phase transition in cosmology [46, 47, 48]. As a result, throughout history

much effort has been put in understanding phase transitions. A crucial step was the development of Landau theory in 1937 [49], which provided a general framework to describe symmetry-breaking phase transitions.

Many phase transitions are associated with spontaneous symmetry breaking of a continuous symmetry [50, 51]. In these transitions the state of the system after the phase transition does not show the same symmetry as the Hamiltonian. As an illustration of spontaneous symmetry breaking, we consider the Heisenberg model for ferromagnetism [52]. In this system the Hamiltonian is invariant under SU(2) symmetry operations, i.e., it is invariant under rotations of the spins. After undergoing the phase transition the spins align in a particular direction and the state of the system breaks spin rotation invariance. However, the original symmetry still has consequences as a global rotation of all spins leaves the energy invariant. Therefore, the ordered phase is infinitely degenerate and spontaneous symmetry breaking by itself does not provide an explanation for which particular ground state the system chooses.

We can investigate this problem by looking at the probability distribution of the quantum-mechanical observable that acquires a nonzero expectation value upon undergoing the transition. In the context of Bose-Einstein condensation, the Hamiltonian is invariant under global $U(1)$ transformations associated with the conservation of the number of atoms. Therefore, the number of condensed particles and the phase of the condensate are conjugate variables. Heisenbergs uncertainty principle implies that for a fixed number of condensed particles the phase of the condensate fluctuates. Thus, in finite-sized condensates the phase is not fixed and the system is not in a state with a definite phase.[1] Rather, the phase of the condensate is characterized by a probability distribution, which can have nontrivial dynamics of its own. It is exactly this nontrivial dynamics of the phase of the condensate which is known as *phase diffusion*.

Phase diffusion was first considered by You and Lewenstein in 1996 in the context of condensates of dilute atomic gases [53, 54]. In the years after its first introduction, considerable theoretical work was done on phase diffusion, as can be found in Refs. [55, 56, 57, 58, 59]. Additionally, there have also been attempts to measure phase diffusion in atomic condensates. In experiments by the groups of Ketterle and Cornell, two independently created Bose-Einstein condensates were made to interfere, resulting in a measurement of the phase difference between the condensates [60, 61]. To measure phase diffusion, however the phase difference should be measured dynamically. Unfortunately, interference experiments with atomic Bose-Einstein condenates are destructive, which means such dynamical measurements are impossible. With a photon Bose-Einstein condensate, the situation is different. As

[1] To understand that a finite size of the condensate is crucial, note that the commutation relation for the conjugate variables is $[\hat{\phi}, \hat{N}] = i\hbar$, with $\hat{\phi}$ the phase operator and $\hat{N}$ the number operator. Applying the number operator to a Fock state will give the number of particles N as an eigenvalue. Thus, in order for the phase operator to obey the commutation relation, the variance $\delta\phi$ of the phase should go as $\delta\phi \sim N^{\alpha}$ with $\alpha < 0$. In the thermodynamic limit this vanishes.

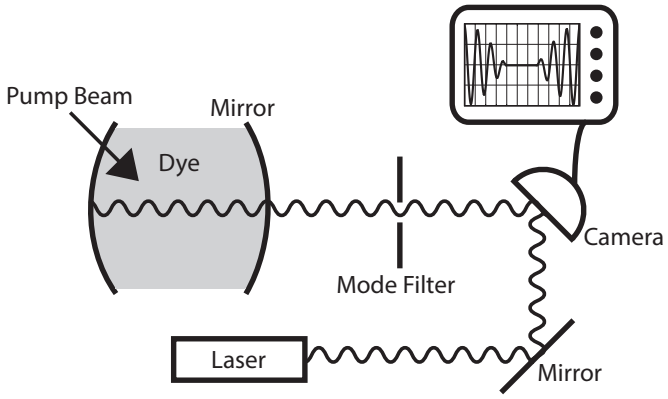

Figure 4.1: Proposal for an experimental setup to measure the phase diffusion of a Bose-Einstein condensate of photons in a dye-filled microcavity. The mode filter selects the condensate mode of the light that leaks through the mirror. These condensed photons interfer with an external laser. By measuring the intensity of the combined signal information is obtained about the phase diffusion of the Bose-Einstein condensate of photons. Image made by Arie-Willem de Leeuw.

the photons continuously escape from the condensate and are replenished by pumping with a laser, one can do interference experiments in a nondestructive manner. In the next section we propose such an experiment.

4.2 Measuring Phase Diffusion

Experimentally, information on the phase of a light source can be determined from a simple interference experiment with another light source. In the case of the photonic condensate, we should simply collect the photons leaving the Bose-Einstein condensate and let them interfere with a reference laser that is tuned close to the eigenfrequency of the cavity. We make sure that only photons from the condensate participate in the interference experiment by guiding the light that comes from the cavity through a mode filter, which lets through only the photons coming from the condensate. This is similar to the experimental situation in Fig. 3.2. By measuring the interference signal with a fast photodiode, the phase diffusion can be directly observed using a spectrum analyzer. A schematic picture of the experimental setup is shown in Fig. 4.1.

The phase diffusion of the condensate is governed by both quantum and thermal fluctuations of the number of condensed particles. Fluctuations are dubbed 'quantum' when they remain present at zero temperature, whereas thermal fluctuations disappear in this limit. Both types of fluctuations contribute to the interference pattern appearing on the screen. In the following, we discuss both contributions separately.

4.2.1 Quantum fluctuations

Let us first consider quantum fluctuations. Since for a finite-size condensate of photons the phase is not well defined, we introduce a density operator $\hat{\rho}$ that takes into account that the photons can be in a superposition of different coherent states with different phases. Following Ref. [21], we write for the intensity of the combined signal of the laser and the condensate at the detector

$$\bar{I}(\mathbf{r},t) = \mathrm{Tr}\left[\hat{\rho}\hat{E}^{-}(\mathbf{r},t)\hat{E}^{+}(\mathbf{r},t)\right], \tag{4.1}$$

where the bar denotes averaging and $\hat{E}^{-}(\mathbf{r},t)$ and $\hat{E}^{+}(\mathbf{r},t)$ indicate the negative and positive frequency part of the sum of the electric field of the laser and the Bose-Einstein condensate. We write

$$\hat{E}^{+}(\mathbf{r},t) = E_L(r)\hat{a}_L e^{i(\mathbf{k}\cdot\mathbf{r}-\omega t)} + E_C(r)\hat{a}_C e^{i(\mathbf{k}\cdot\mathbf{r}-\omega t)}, \tag{4.2}$$

with $E_L(r)$ the norm of the electric field of the laser, $E_C(r)$ the norm of the electric field of the photon beam coming from the condensate, $\hat{a}_L$ and $\hat{a}_C$ the annihilation operators for the laser and condensate, ω the frequency of the condensate and laser and finally $\mathbf{k}$ the corresponding wave number. Additionally, $\hat{E}^{-}(\mathbf{r},t)$ is given by the complex conjugate of Eq. (4.2). Note that we have assumed that the radial distances from respectively the laser or the condensate to the detector are the same and that the laser is frequency-locked to the condensate. These conditions simplify the following equations significantly, but can be reintroduced easily when necessary.

For our system the relevant basis states are the coherent states $|\theta_\mathrm{C}\rangle \otimes |\theta_\mathrm{L}\rangle$, where $|\theta_\mathrm{L}\rangle$ is a coherent state of the laser with phase θ_L and $|\theta_\mathrm{C}\rangle$ a coherent state of the Bose-Einstein condensate with a certain phase θ. Note that we consider these product states as the photons from the laser and the Bose-Einstein condensate are reasonably assumed to be independent. Due to the properties of coherent states, we have

$$\begin{aligned}\hat{a}_L|\theta_C\rangle \otimes |\theta_L\rangle &= \rho_L e^{i\theta_L}|\theta_C\rangle \otimes |\theta_L\rangle \\ \hat{a}_C|\theta_C\rangle \otimes |\theta_L\rangle &= \rho_C e^{i\theta}|\theta_C\rangle \otimes |\theta_L\rangle\end{aligned} \tag{4.3}$$

where ρ_L and ρ_C represent the amplitude of the coherent states of the laser and the condensate. We proceed by assuming that the laser is in a pure state. However, the photons coming from the condensate are in a mixed state as the global phase of the condensate is not well defined. Therefore, the density operator is given by [62]

$$\hat{\rho} = \int_0^{2\pi} \mathrm{d}\theta P(\theta,t)|\theta_C\rangle \otimes |\theta_L\rangle\langle\theta_L| \otimes \langle\theta_C|e^{-|\rho_C|^2}e^{-|\rho_L|^2}, \tag{4.4}$$

where $P(\theta,t)$ is the probability for the Bose-Einstein condensate to have phase θ at a time t, i.e., $P(\theta) = |\Psi(\theta,t)|^2$, for a wavefunction $\Psi(\theta,t)$ which describes the quantummechanical evolution of

the phase as a function of time. Since the probability is normalized, we have $\mathrm{Tr}[\hat{\rho}] = 1$. By using the properties in Eq. (4.3), we obtain for the intensity

$$\begin{aligned}\bar{I}(\mathbf{r},t) &= \int_0^{2\pi} \mathrm{d}\theta P(\theta,t)\langle\theta_L| \otimes \langle\theta_C|\hat{E}^-(\mathbf{r},t)\hat{E}^+(\mathbf{r},t)|\theta_C\rangle \otimes |\theta_L\rangle \\ &:= I_L(\mathbf{r},t) + I_C(\mathbf{r},t) + \bar{I}_{\mathrm{I}}(\mathbf{r},t),\end{aligned} \tag{4.5}$$

where $I_L(\mathbf{r},t) = E_L^2(r)\rho_L^2$, $I_C(\mathbf{r},t) = E_C^2(r)\rho_C^2$ and the interference contribution to the intensity reads

$$\bar{I}_{\mathrm{I}}(\mathbf{r},t) = 2A_{\mathrm{I}}(\mathbf{r},t)\int_0^{2\pi} \mathrm{d}\theta P(\theta,t)\cos\theta, \tag{4.6}$$

where we set the phase $\theta_L = 0$ without any loss of generality and defined $A_{\mathrm{I}}(\mathbf{r},t) := E_L(r)E_C(r)\rho_L\rho_C$. Since the intensity of the photons coming from the condensate is independent of the phase, this interference part of the intensity is the only relevant contribution for observing phase diffusion. In order to calculate a typical interference pattern from Eq. (4.6), we need an explicit expression for the probability distribution $P(\theta,t)$ for the phase of the condensate. We calculate this probability distribution by quantizing a field theory in Section 4.3. However, first we consider phase diffusion due to thermal fluctuations in the next section.

4.2.2 Thermal Fluctuations

Similar to the description of Brownian motion in statistical physics, we describe the thermal fluctuations of the phase of the condensate by a Langevin equation. In fact, as the phase of the condensate and number of particles in the condensate are conjugate variables, we need two Langevin equations. These equations, also known as stochastic equations of motion, are coupled. For now, we postpone the derivation of these Langevin equations to Section 4.6.

As the description of the thermal fluctuations is different from the quantum fluctuations, we need to modify our expression for the interference pattern. In the previous section we found an expression by taking the average over an ensemble consisting of various quantum states, each with a certain probability. A single experimental measurement, however, typically yields

$$I_{\mathrm{I}}(\mathbf{r},t) = 2A_{\mathrm{I}}(\mathbf{r},t)\cos(\theta(t)), \tag{4.7}$$

where $\theta(t)$ is the solution to the relevant stochastic equations of motion, for one realization of the noise. As mentioned before, the fluctuations of the phase of the condensate are only present in this interference part of the intensity and therefore we are primarly interested in this part of the intensity. Additionally, note that every realization of the noise results into a different interference pattern, and therefore every individual measurement will give a different result. In order to extract information on

the phase diffusion of the condensate due to thermal fluctuations, we should average Eq. (4.7) over all configurations of the noise. Using the Langevin equations we motivate in Section 4.6, we perform this averaging in Section 4.7.

Now that we know how the interference pattern due to both thermal and quantum flucutations depends on the phase, we proceed with looking at phase diffusion due to quantum fluctuations by deriving the probability distribution for the phase in the next section.

4.3 Phase Probability Distribution

For an explicit expression of the intensity Eq. (4.6) as a function of time, we need to determine the probability $P(\theta, t)$. In analogy with Ref. [36], we obtain this probability by quantizing a field theory that describes the dynamics of the phase of a Bose-Einstein condensate of photons. Again we describe the photons as an interacting Bose gas in a two-dimensional isotropic harmonic trapping potential with frequency ω. Recall that the photons have a constant zero-momentum energy mc^2, with c the speed of light in the medium. Note that we have assumed the laser to be frequency locked to mc^2. Therefore, in imaginary time the relevant action of the bosonic photon fields $\phi(\mathbf{x}, \tau)$ is given by[2]

$$S[\phi^*, \phi] = \int_0^{\hbar\beta} \mathrm{d}\tau \int \mathrm{d}\mathbf{x}\ \phi^*(\mathbf{x}, \tau)\left(\hbar\frac{\partial}{\partial\tau} - \frac{\hbar^2\nabla^2}{2m} + \frac{1}{2}m\omega^2|\mathbf{x}|^2 - \mu + \frac{g}{2}|\phi(\mathbf{x}, \tau)|^2\right)\phi(\mathbf{x}, \tau), \quad (4.8)$$

where $\mathbf{x} = (x, y)$ is the two-dimensional position, g is the interaction strength and μ is the chemical potential of the system. Note the similarities with Eq. (3.1), which we used to derive the probability distribution for the number of particles in the condensate. In order to make the phase of the condensate appear explicitly, we use the variable transformation $\phi(\mathbf{x}, \tau) = \sqrt{\rho(\mathbf{x}, \tau)}e^{i\theta(\mathbf{x},\tau)}$, where $\rho(\mathbf{x}, \tau)$ represents the density of the system and $\theta(\mathbf{x}, \tau)$ the phase of the condensate. In terms of these new fields the action reads

$$S[\rho, \theta] = \int_0^{\hbar\beta} \mathrm{d}\tau \int \mathrm{d}\mathbf{x}\ \left[i\hbar\rho(\mathbf{x}, \tau)\frac{\partial\theta(\mathbf{x}, \tau)}{\partial\tau} + \frac{\hbar^2\rho(\mathbf{x}, \tau)}{2m}|\nabla\theta(\mathbf{x}, \tau)|^2 + \frac{\hbar^2}{8m\rho(\mathbf{x}, \tau)}|\nabla\rho(\mathbf{x}, \tau)|^2 + \left(\frac{1}{2}m\omega^2|\mathbf{x}|^2 - \mu\right)\rho(\mathbf{x}, \tau) + \frac{g}{2}\rho^2(\mathbf{x}, \tau)\right]. \quad (4.9)$$

Due to the coupling between the density and phase field, we need to integrate out the density field $\rho(\mathbf{x}, \tau)$ to extract the dynamics of the phase of the condensate. This can be done exactly in the Thomas-Fermi limit, which we introduced in Section 3.3. Thus, we neglect the kinetic terms in the action, i.e., $\nabla\rho(\mathbf{x}, \tau)$ and $\nabla\theta(\mathbf{x}, \tau)$. We stress again that this approximation is valid only if the

[2] In Chapter 3 we started from an action over all space and spend some time explicitly separating the longitudinal and transverse part of the photon field. Here we immediately consider only the two-dimensional transverse photon field. The coupling constant g is assumed to be scaled appropriately.

interaction energy is much more important than the kinetic energy. We obtain

$$S[\rho,\theta] \approx \int_0^{\hbar\beta} \mathrm{d}\tau \int \mathrm{d}\mathbf{x} \left[i\hbar\rho(\mathbf{x},\tau)\frac{\partial\theta(\mathbf{x},\tau)}{\partial\tau} + \left(\frac{1}{2}m\omega^2|\mathbf{x}|^2 - \mu\right)\rho(\mathbf{x},\tau) + \frac{g}{2}\rho^2(\mathbf{x},\tau)\right]. \quad (4.10)$$

Recall that we derived the Thomas-Fermi equilibrium density profile $\langle\rho(\mathbf{x})\rangle$ and also the associated Thomas-Fermi radius $R_{\mathsf{TF}} = (4gN_0/\pi m\omega^2)^{1/4}$ in Eqs. (3.6) and (3.7) in Section 3.3. Using these results, we perform a fluctuation expansion $\rho(\mathbf{x},\tau) = \langle\rho(\mathbf{x})\rangle + \delta\rho(\mathbf{x},\tau)$ in the action, yielding

$$S[\rho,\delta\rho,\theta] = \int_0^{\hbar\beta} \mathrm{d}\tau \int \mathrm{d}\mathbf{x} \left[i\hbar\left(\langle\rho(\mathbf{x})\rangle + \delta\rho(\mathbf{x},\tau)\right)\frac{\partial\theta(\mathbf{x},\tau)}{\partial\tau} + \frac{g}{2}\left(\delta\rho^2(\mathbf{x},\tau) - \langle\rho(\mathbf{x})\rangle^2\right)\right]. \quad (4.11)$$

Subsequently, we split the square in the previous result and integrate out the density fluctuations to find

$$S^{\mathsf{eff}}[\rho,\theta] = \int_0^{\hbar\beta} \mathrm{d}\tau \int_{A_{\mathsf{TF}}} \mathrm{d}\mathbf{x}\left[i\hbar\langle\rho(\mathbf{x})\rangle\frac{\partial\theta(\mathbf{x},\tau)}{\partial\tau} + \frac{\hbar^2}{2g}\left(\frac{\partial\theta(\mathbf{x},\tau)}{\partial\tau}\right)^2\right], \quad (4.12)$$

where we omitted irrelavant shifts in the action, which are not a function of the phase. Furthermore, note that the spatial integral in the expression above is restricted to the Thomas-Fermi area, given by $A_{\mathsf{TF}} = \pi R_{\mathsf{TF}}^2$, as the average density profile is only defined in this region of space.

To proceed, we split the phase in a position-independent and position-dependent part, i.e., $\theta(\mathbf{x},\tau) = \theta_0(\tau) + \theta_1(\mathbf{x},\tau)$. As the photons in the condensate occupy the ground state, we are mostly interested in the global $U(1)$-part of the action, given by $S[\theta_0]$. Retaining only this global part, omitting the subscript on θ_0 and subsequently performing a Wick rotation $\tau \to it$ yields

$$S^{\mathsf{eff}}[\theta] = \int \mathrm{d}t\left[\frac{A_{\mathsf{TF}}\hbar^2}{2g}\left(\frac{\mathrm{d}\theta(t)}{\mathrm{d}t}\right)^2 - \hbar N_0\frac{\mathrm{d}\theta(t)}{\mathrm{d}t}\right] := \int \mathrm{d}t\mathcal{L}[\dot\theta], \quad (4.13)$$

with $N_0 = \int_{A_{\mathsf{TF}}} \mathrm{d}\mathbf{x}\langle\rho(\mathbf{x})\rangle$ the number of particles in the condensate. Note that the Wick rotation amounts to $\exp\left(-\int \mathrm{d}\tau\mathcal{L}/\hbar\right) \to \exp\left(i\int \mathrm{d}t\mathcal{L}/\hbar\right)$, such that we had to extract an overal factor of $-i$ in going from Eq. (4.12) to Eq. (4.13).

Summarizing, the treatment above has given us an effective action in real time for the global $U(1)$-part of the action associated with an interacting Bose gas in a harmonic trapping potential, in the Thomas-Fermi limit. We proceed by calculating the conjugate momentum p_θ associated to the Lagrangian in Eq. (4.13) and find the Hamiltonian $\mathcal{H}$ of the system

$$\mathcal{H} = \frac{g}{2A_{\mathsf{TF}}\hbar^2}\left(p_\theta + \hbar N_0\right)^2. \quad (4.14)$$

Now we quantize the system by imposing the canonical commutation relation $[\theta, p_\theta] = i\hbar$, resulting in $p_\theta = -i\hbar\partial/\partial\theta$. The Schrödinger equation for the phase θ is then found to be

$$i\hbar\frac{\partial\Psi(\theta,t)}{\partial t} = -D\left(\frac{\partial}{\partial\theta} + iN_0\right)^2\Psi(\theta,t), \quad (4.15)$$

where we defined the "diffusion constant"[3] $D := g/2\pi R_{\mathrm{TF}}^2$. with R_{TF} the Thomas-Fermi radius of the condensate. We derive the general solution to this Schrödinger equation for the phase in Appendix B.1 and it reads

$$\Psi(\theta,t) = \sum_{n\in\mathbb{Z}} c_n \exp\left(-\frac{iD(n+N_0)^2 t}{\hbar} + in\theta\right), \tag{4.16}$$

where the coefficients c_n are determined by the initial condition of the wavefunction. In the next section we shall assume a strongly peaked initial wavefunction to calculate these coefficients. Subsequently, we calculate and plot a typical interference pattern due to the quantum fluctuations.

4.4 Interference due to Quantum Fluctuations

In order to demonstrate the phase diffusion due to quantum fluctuations and to calculate a typical interference pattern, we consider the example that the initial wavefunction is a superposition of Gaussians centered around $\theta = 0 \bmod 2\pi$,

$$\Psi(\theta,0) = \frac{1}{(\pi\sigma^2)^{1/4}} \sum_{n\in\mathbb{Z}} \exp\left(-\frac{(\theta+2\pi n)^2}{2\sigma^2}\right). \tag{4.17}$$

Taking this superposition ensures that the wavefunction is periodic, i.e., $\Psi(\theta,0) = \Psi(\theta+2\pi,0)$. In principle we have a slightly different normalization factor, but for the small values of $\sigma < 1$ considered here, this is a very good approximation. In experiments one would measure the phase of the condensate, thus letting the wave function collapse, and then subsequently look at its dynamics. Hence, we start from a wavefunction that is strongly peaked and therefore we can use in good approximation that $\sigma < 1$.

For this initial wavefunction, we can determine c_n exactly and obtain an analytic expression for the wavefunction at a time t. We show in Appendix B.2 that it reads

$$\Psi(\theta,t) = \left(\frac{\sigma^2}{4\pi^3}\right)^{1/4} \sum_{n\in\mathbb{Z}} \exp\left(-\frac{iD(n+N_0)^2 t}{\hbar} + in\theta - \frac{n^2\sigma^2}{2}\right). \tag{4.18}$$

Using this wavefunction, we calculate the probability $P(\theta,t) = |\Psi(\theta,t)|^2$. Typical plots of this probability are shown in Fig. 4.2. At $t = 0$ we have a sharp peak and therefore the phase of the condensate is well defined. However, if time evolves the peak smears out and moves its position in time. As time evolves even further, the probability regains its original shape. This phenomenon is known as collapse and revival of the wavefunction, which was recently observed in a somewhat different context [63]. It

[3] We use quotation marks because it has units of energy J instead of the more common units m·s^{-2} for a diffusion constant.

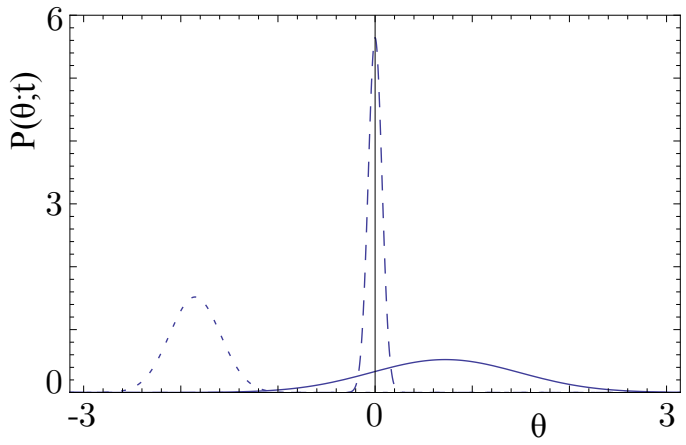

Figure 4.2: The probability $P(\theta, t)$ for the phase of the Bose-Einstein condensate of photons at different times for $N_0 = 5 \cdot 10^4$ and $\sigma = 10^{-1}$. The dashed, dotted and solid curve are the probability at $t = 0$, $t = t_0$ and $t = 3t_0$ with $t_0 := \hbar/D\sqrt{N_0} = \sqrt{16\pi/\tilde{g}\omega^2}$. We clearly see the diffusion of the phase of the condensate as time evolves.

is a direct consequence of the invariance of the wavefunction for $t \to t + 2\pi k\hbar/D$ for every integer k, as can be deduced from Eq. (4.16). Hereafter, cycles of collapse and revival of the wavefunction occur.

Moreover, we use our expression for the probability to obtain the average interference pattern as defined in Eq. (4.6). Again for small $\sigma < 1$, we find in Appendix B.3 that

$$\bar{I}_{\mathrm{I}}(\mathbf{r}, t) \approx \frac{4\sigma A_{\mathrm{I}}(\mathbf{r}, t)}{\sqrt{\pi}} \cos\left(\frac{5(1+2N_0)\sigma t}{2t_{\mathrm{col}}}\right) \sum_{n\in\mathbb{Z}} \cos\left(\frac{5n\sigma t}{t_{\mathrm{col}}}\right) e^{-n(n+1)\sigma^2}, \tag{4.19}$$

with $t_{\mathrm{col}} = 5\hbar\sigma/2D$. In fact, this can be simplified even further under the assumption of small σ to yield

$$\bar{I}_{\mathrm{I}}(\mathbf{r}, t) \approx 4A_I(\mathbf{r}, t) \cos\left(\frac{5(1+2N_0)\sigma t}{2t_{\mathrm{col}}}\right) \exp\left(-\frac{25t^2}{t_{\mathrm{col}}^2}\right). \tag{4.20}$$

A typical plot of an interference pattern is displayed in Fig. 4.3. The time scale t_{col} gives a measure of the time needed for this pattern to vanish for the first time. Furthermore, this expression contains two other important time scales. The first scale is the oscillation time of the intereference pattern, which for a relatively large number of condensed photons $N_0 \gg 1$ is given by $t_{\mathrm{osc}} = \hbar/2DN_0$. By using the relation $\mu = m\omega^2 R_{\mathrm{TF}}^2/2$, valid in the Thomas-Fermi limit, one shows that $D = (1/2)(\partial\mu/\partial N_0)$, such that $t_{\mathrm{osc}} = 2\hbar/\mu$. Physically, this is the well-known AC Josephson effect. The additional factor of two comes from the fact that we effectively performed an expansion of the grand-canonical energy around the average number of particles up to second order in Section 4.3. By resummation up to all orders, one shows that in fact $t_{\mathrm{osc}} = \hbar/\mu$, which is the result we shall continue to use.

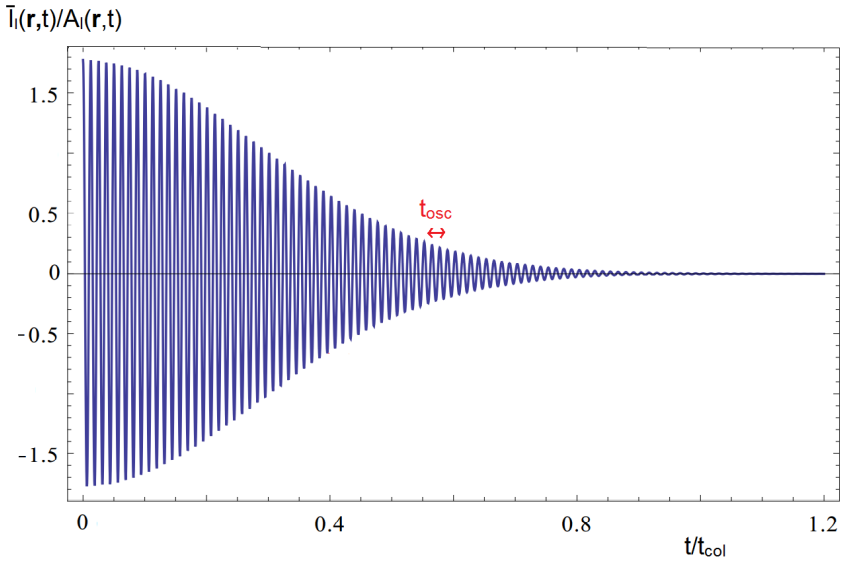

Figure 4.3: Typical plot of the interference pattern from Eq. (4.19) due to quantum fluctuations as a function of the time scale $t_{\rm col}$ for $N_0 = 10^3$. The high-frequency behavior has frequency $1/t_{\rm osc}$, whereas the envelop function decays over the time scale $t_{\rm col}$. The time scale of revival $t_{\rm rev}$ is too long to be visible in this plot.

The second time scale, given by $t_{\rm rev} = 2\pi\hbar/D$, is the revival time for which the interference pattern returns to its original shape. Note that this time scale is larger than $t_{\rm osc}$ by a factor of $4\pi N_0$. Furthermore, in the thermodynamic limit $N_0 \to \infty$, we find that $D \propto 1/\sqrt{N_0} \to 0$ and both $t_{\rm col} \to \infty$ and $t_{\rm rev} \to \infty$. Hence, in the thermodynamic limit the condensate can be described as a symmetry-broken phase, such that no phase diffusion occurs.

In the next section we again consider the interference pattern due to quantum fluctuations. However, this time we include the effects of dissipation due to the self-interaction of the photons with the heat bath of dye molecules.

4.5 Interference due to Quantum Fluctuations with Damping

In the previous calculations we have ignored that the photons are confined to a dye-filled optical microcavity and that there is dissipation through the interaction with these dye molecules. As is shown in Ref. [42], for low energies these interaction effects can in very good approximation be represented by one single dimensionless damping parameter α. To incorporate this damping into our calculation, we note that damping results into finite lifetimes for states with a nonzero energy. Therefore, as a

first attempt to include dissipation, we change Eq. (4.16) into

$$\Psi(\theta,t)=\sum_{n\in\mathbb{Z}}c_n\int_{-\infty}^{\infty}\mathrm{d}E\,\rho(E,n)\exp\left(-\frac{iEt}{\hbar}+in\theta\right), \tag{4.21}$$

where we introduced a spectral function $\rho(E,n)$, given by

$$\rho(E,n)=\frac{1}{\pi}\frac{\alpha E}{(E-D(n+N_0)^2)^2+\alpha^2E^2}. \tag{4.22}$$

Note that $\lim_{\alpha\to0}\rho(E,n)=\delta(E-D(n+N_0)^2)$, such that in the limit of negligible damping Eq. (4.21) reduces to the original expression Eq. (4.16). Also, note that a consequence of approximating the dissipation effects with its low-energy limit is a violation of the sum rule, since the integral of the spectral function over all energies gives $1/(1+\alpha^2)$. However, the experimental value of α is rather small and therefore this approximation only leads to a small deviation [42].

We proceed by calculating the integral in Eq. (4.22) by contour integration and subsequently follow the same steps as in Appendix B.3. For a relatively small number of condensed photons and upon neglecting terms of order α^2, the interference pattern with dissipation ultimately reads

$$\bar{I}(\mathbf{r},t;\alpha)\simeq e^{-t/t_{\mathrm{dis}}^{(1)}}\bar{I}_{\mathrm{I}}(\mathbf{r},t), \tag{4.23}$$

where $t_{\mathrm{dis}}^{(1)}=\hbar/4\alpha DN_0^2$ and $\bar{I}_{\mathrm{I}}(\mathbf{r},t)$ is given by Eq. (4.19). Thus with dissipation there is another time scale $t_{\mathrm{dis}}^{(1)}$, which indicates the decay time of the interference pattern. One shows that $t_{\mathrm{dis}}^{(1)}/t_{\mathrm{col}}=1/10\alpha\sigma N_0^2$, such that the shortest decay time scale is determined by the number of particles in the condensate N_0. Note that for very large condensates $N_0\gg1$, the low-energy approximation of the dissipation is no longer valid and we have to incorporate the complete energy dependence of the photon decay rate $\Gamma(E)$ as calculated in Ref. [42]. In good approximation the dissipation time scale is then found by replacing αDN_0^2 by $\hbar\Gamma(DN_0^2)/2$. In practice this means that for large condensate fractions, the dissipative time scale due to quantum fluctuations becomes too large to be observable experimentally.

This section concludes our study of the contribution of quantum fluctuations to the interference pattern. In the next sections we derive the necessary stochastic equations to describe thermal fluctuations of the condensate parameters.

4.6 Stochastic Equations

The Gross-Pitaevskii equation is a mean-field equation which describes the average dynamics of a Bose-Einstein condensate. In order to describe the nonequilibrium dynamics of a condensate, we have to go beyond a mean-field description. The theory for this is developed in Refs. [64, 65]. Here we only

cite the most important conclusions.

By using Keldysh theory and employing the so-called many-body T-matrix approximation, one derives that the probability distribution $P[N,\theta,t]$ for the number of particles N and phase θ of a condensate at a time t is given as a functional integral by

$$P[N,\theta;t] = \int_{\theta(t)=\theta}^{N(t)=N} \mathrm{d}[N]\,\mathrm{d}[\theta]\exp\left(\frac{i}{\hbar}S^{\mathrm{eff}}[N,\theta]\right), \tag{4.24}$$

with the effective action

$$S^{\mathrm{eff}}[N,\theta] = \int_{t_0}^{t}\mathrm{d}t'\left[\frac{2N(t')}{\hbar\Sigma^K}\left(\hbar\dot{\theta}(t')-\mu\right)^2 + \frac{\hbar}{2\Sigma^K N(t')}\left(\dot{N}(t')+\frac{2R}{\hbar}N(t')\right)^2\right]. \tag{4.25}$$

In this action the condensate chemical potential μ is redefined to include interaction effects, Σ^K is the Keldysh self-energy and R is the imaginary part of the retarded self-energy that describes the exchange of bosons between the condensate and the thermal cloud. In fact, the last two quantities are related via

$$\hbar\Sigma^K(\mathbf{k},\omega) = -2i[1+2N_{\mathrm{BE}}(\hbar\omega)]R(\mathbf{k},\omega), \tag{4.26}$$

with $N_{\mathrm{BE}}(x) := (e^{\beta x}-1)^{-1}$ the Bose distribution. The interaction of the photons with the molecules can be described by one dimensionless parameter α, as is derived in Ref. [42]. This means that we have $R(\mathbf{k},\omega) = -i\alpha\hbar\omega$. Since we are dealing with Bose-Einstein condensation, we can also use the fluctuation-dissipation theorem for large occupation numbers, meaning that we may approximate $1+2N_{\mathrm{BE}}(\hbar\omega) \simeq 2/\beta\hbar\omega$. Because the photons are at room temperature, we expect this to be a very good approximation. Substituting these approximations into Eq. (4.26), we obtain $\hbar\Sigma^K(\mathbf{k},\omega) = -4i\alpha/\beta$.

We proceed by performing two Hubbard-Stratonovich transformations on the path integral in Eq. (4.24), one for the global phase θ and one for the number of particles N in the condensate. By again following the lines of Ref. [65] we find up to first order in α

$$\begin{cases} \hbar\dot{\theta}(t) = -\mu + \nu(t)/\sqrt{N(t)}, \\ \hbar\dot{N}(t) = -2\alpha\mu N(t) + 2\hbar\sqrt{N(t)}\eta(t), \end{cases} \tag{4.27}$$

where the stochastic generalized forces $\eta(t)$ and $\nu(t)$ are Gaussian and obey

$$\begin{cases} \langle\nu(t)\rangle = \langle\eta(t)\rangle = \langle\eta(t)\nu(t')\rangle = 0, \\ \langle\nu(t)\nu(t')\rangle = \hbar^2\langle\eta(t)\eta(t')\rangle \simeq \alpha\hbar\beta^{-1}\delta(t-t'). \end{cases} \tag{4.28}$$

Note that the strength of the noise for the number $N(t)$ and phase $\theta(t)$ of the condensed photons scales differently with the number of condensed photons. For larger number of photons the fluctuations

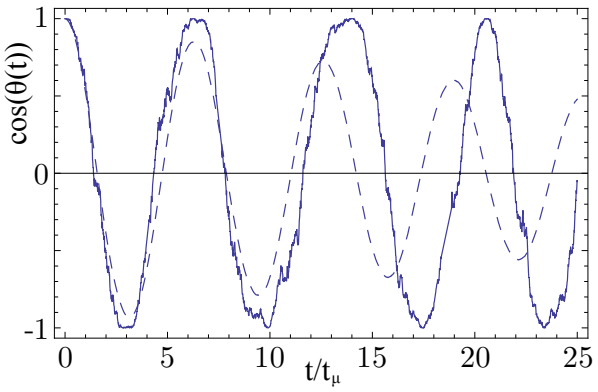

Figure 4.4: The result of $\cos(\theta(t))$ as a function of $t/t_{\rm osc}$ with $t_{\rm osc} = \hbar/\mu \simeq 5 \cdot 10^{-10}\,{\rm s}$. Here $\theta(t)$ is a solution to the Langevin equation describing the dynamics of the phase of the condensate for $N(t) = \langle N \rangle = 4 \cdot 10^4$, $\alpha = 10^{-1}$ and $\hbar\beta \simeq 2.5 \cdot 10^{-14}\,{\rm s}$. The solid curve is the result for an arbitrary noise configuration and the dashed curve represents the average over 500 different configurations of the noise.

in the particle number increase, but the fluctuations in the global phase decrease. Moreover, in the thermodynamic limit the noise for the global phase vanishes and we obtain again a condensate with a well-defined phase.

Now that we have obtained the necessary Langevin equations, we proceed by evaluating the interference pattern due to thermal fluctuations in the next section.

4.7 Interference due to Thermal Fluctuations

To highlight the fluctuations of the phase due to thermal fluctuations we would like to minimize the fluctuations in the intensity of the external laser and the light coming from the condensate. Since the intensity of the condensate is proportional to the number of condensed photons, we are interested in the regime with small number fluctuations. As can be deduced from the discussion in Chapter 3 and Eqs. (4.27), the number fluctuations decrease for increasing condensate fractions. Therefore, we consider large condensate fractions such that the fluctuations in the interference pattern are dominated by phase fluctuations, and we take $N(t) = \langle N(t) \rangle := N_0$.

In Fig. 4.4 we show the result for $\cos(\theta(t))$, where $\theta(t)$ is a solution to the stochastic Eqs. (4.27) for a condensate fraction of roughly $35\,\%$. The solid curve gives the interference pattern for a certain realization of the stochastic forces. Every realization of the noise results into a different interference pattern, and therefore every individual measurement will give a different result. However, once we average over more and more noise realizations $\langle \cos(\theta(t)) \rangle$ converges, and we do observe the decay associated with the dissipation.

In order to get more information about this decay of the intensity $I_{\rm I}(\mathbf{r},t)$, we have to take the average of Eq. (4.7) over all noise configurations. By using the Fokker-Planck equation as derived in Ref. [65], we find up to first order in α

$$\begin{cases} \hbar\dfrac{\partial}{\partial t}\langle\cos(\theta)\rangle &= \mu\langle\sin(\theta)\rangle - \dfrac{\alpha}{2\beta N_0}\langle\cos(\theta)\rangle, \\ \hbar\dfrac{\partial}{\partial t}\langle\sin(\theta)\rangle &= -\mu\langle\cos(\theta)\rangle - \dfrac{\alpha}{2\beta N_0}\langle\sin(\theta)\rangle. \end{cases} \tag{4.29}$$

These equations admit analytic solutions and we find for the average of the interference part of the intensity

$$\langle I_{\rm I}(\mathbf{r},t)\rangle = 2A_{\rm I}(\mathbf{r},t)\exp\left(-\frac{\alpha t}{2\hbar\beta N_0}\right)\cos\left(\frac{\mu t}{\hbar}\right), \tag{4.30}$$

which coincides with the result in Fig. 4.4 where we averaged over 500 noise realizations. Again we observe two relevant time scales in the expression above. The first is the dissipative time scale in the exponential $t_{\rm dis}^{(2)} = 2\hbar\beta N_0/\alpha$, whereas the second is the characteristic oscillation time of the cosine $t_{\rm osc} = \hbar/\mu$. Note that this latter time scale is again a manifestation of the AC Josephson effect, similar to what we found in Section 4.4.

For typical values for the trap frequencies ω, we obtain that $t_{\rm osc}$ is in the order of picoseconds. Since this is rather small, we expect that it is challenging to measure these oscillations experimentally. However, it might be possible to measure one of the other time scales we have found in this chapter. Realistic experimental parameters are large condensate numbers $N_0 \gg 1$ and α ranging from 10^{-1} to 10^{-2}. As discussed in Section 4.5, the time scale $t_{\rm dis}^{(1)}$, which describes dissipative effects due to quantum fluctuations, diverges for large condensate numbers. It is therefore not measurable in a typical experimental setup. Fortunately, the decay time due to thermal fluctuations $t_{\rm dis}^{(2)}$ is in the nanoseconds regime, which is within the precision of current devices.

4.8 Conclusion

We have proposed an interference experiment of condensed photons with an external laser to observe phase diffusion experimentally. Furthermore, we have shown that the typical outcome of individual experiments can be obtained from a stochastic equation for the phase of the condensate. Additionally, we have demonstrated that thermal fluctuations dominate and we found that the decay time of the average interference pattern is in the nanosecond regime, which is an accessible time scale in experiments. Finally we note that although the calculations in this chapter are specific for a Bose-Einstein condensate of photons, the concepts and ideas presented are also applicable to Bose-Einstein condensates of exciton-polaritons. Also in these condensates we can get experimental information about the

global phase of the condensate. For example, in Refs. [66, 67] the relative global phase of two coupled exciton-polariton condensates is measured in order to investigate Josephson oscillations.

Chapter 5

Discussion and Outlook

In this final chapter we first recapitulate all results and conclusions from this Thesis. Subsequently, we consider work in progress and what might be interesting to look at next.

5.1 Results of this Thesis

The main goal of this Thesis was to advance the theoretical description of a Bose-Einstein condensate of photons. We built upon the theory developed by the experimentalists of Bonn university and also upon previous work performed in our research group. In the process we kept a close eye on recent experiments and also on new experimental possibilities.

We started by noting in Chapter 1 that over the past decade different condensates of bosonic quasiparticles have been created, among which a condensate of massive photons. These condensates of quasiparticles are different from the 'traditional' condensates of dilute atomic vapors, e.g., they can be created at higher temperatures and are in a steady state, but not in a true equilibrium. The main problem in creating a condensate of photons is to find a number-conserving thermalization process, i.e., a way to tune the photon number and temperature of a photon gas independently. In Chapter 2 we discussed in detail the experimental setup used to create the first condensate of photons. Number-conserving thermalization is made possible by confining photons in a dye-filled microcavity. Theoretically, we described the photons in the cavity as particles with an effective mass in a harmonic trapping potential. Additionally, due to imperfect cavity mirrors, photons leak from the cavity. This yields a diagnostic tool 'for free': one simply collects photons leaking from the cavity and performs an analysis on this signal. This situation is in stark contrast to measurements on atomic condensates, which are often destructive. It is this aspect of the experimental realization of a condensate of photons

which allows for new kinds of experiments as compared to the experiments on atomic condensates. On the other hand, the specific experimental realization of the Bonn condensate of photons also brings about certain limitations. For instance, the harmonic trapping frequency is determined by the radius of curvature of the mirrors and the mirror separation. In order to change this frequency, one has to change the experimental setup itself. An electronic mechanism to be able to change the trapping frequency continuously would be more useful.

The measurements on large number fluctuations in a condensate of photons motivated our investigations in Chapter 3. We presented a general theory to calculate number flucutations in harmonically trapped Bose-Einstein condensates. We specialized to two dimensions, but the calculation can be performed in any dimension. The crucial ingredient was the introduction of a four-point vertex in the energy functional of the harmonically trapped Bose gas. Using the probability distribution for the number of photons in the condensate, we were able to quantitatively describe recent experiments on the photonic condensate. Firstly, we could reproduce any experimental curve of the photon number probability as a function of the photon number, for any condensate fraction, by simply using the interaction strength as a fitting parameter. Secondly, we reproduced all curves of the zero-time delay autocorrelation function as a function of the condensate fraction for different dyes, again by using the interaction strength as a fitting parameter. Interestingly, the only available experimental result on the dimensionless interaction strength coincided well with one of our fits to experimental data points which were obtained in similar circumstances to that one measurement. This suggest that interactions play an important role in condensate number fluctuations.

Subsequently, we tried to uncover the microscopic origin of the photon-photon contact interaction in a condensate of photons. Experiments indicate that the mechanism must depend on the type of dye molecules, as well as the concentration of the dye solution. Possible mechanisms we considered were thermal lensing and nonlinear effects. In the literature, the former effect is considered to be most important. However, we modeled it by treating temperature fluctuations diffusively and found that it is too small. Additionally, it does not depend on the dye in any way. As a possible solution, we proposed dye-mediated photon-photon scattering. This mechanism does depend on the dye, but was also found to be too small. This may be the case because we heavily simplified the difficult dye molecules to a simple two-level system.

Thus, we concluded that systematic measurements of the interaction strength are necessary to understand the true nature of the interaction. These experiments are very important, since if the interaction is indeed a contact interaction at long wavelengths, then this would imply that the photon condensate is also a superfluid. Additionally, knowing the microscopic mechanism might give the powerful possibility to tune the photon-photon interactions, similar to the usage of Feshbach resonances in experiments on Bose-Einstein condensates of dilute atomic vapors.

In Chapter 4 we switched from explaining recent experiments to proposing a new type of experiment. Phase diffusion is the phenomenon that the global phase of a finite-sized condensate has a nontrivial dynamics in time. We proposed an interference experiment of condensed photons with an external laser to observe phase diffusion experimentally. For this type of experiment, we calculated interference patterns due to quantum fluctuations and thermal fluctuations separately. In the process we found several time scales. One of these causes a high-frequency oscillation in the interference pattern and can be identified as the AC Josephson effect. For reasonable experimental parameters these oscillations are of the order of picoseconds. This makes them out of reach for current-day experiments. Additionally, we found several collapse time scales, on which the interference pattern vanishes for the first time. The question is if the shortest of these time scales is long enough to be measurable experimentally. Indeed, we estimated that the collapse time due to thermal fluctuations is of the order of nanoseconds, making it measurable using today's machinery.

Next, we briefly discuss work which is not part of this Thesis, but is already under way.

5.2 Work in Progress

We already mentioned that if the photon-photon interaction from Chapter 3 is a contact interaction at long wavelengths, then this would imply that the photon condensate is also a superfluid. However, an important question is how to prove this experimentally. A well-known smoking gun for superfluidity is the observation of quantized vortices. Indeed, quantized vertices were observed in an ultracold vapor of ^{87}Rb by 'stirring' it with a laser, proving it is also a superfluid [68]. However, it is very challenging, if not impossible, to perform a similar experiment in the dye-filled optical microcavity used to create a condensate of photons.[1]

In fact, there is another smoking gun related to superfluidity in a Bose-Einstein condensate. When one suddenly rotates the eigenaxes of a harmonically trapped Bose gas around a small angle, the gas starts to perform an oscillation around the new axes. In the case of an anharmonic trapping potential, the condensate can oscillate in the so-called *scissor mode*. The resonant frequency of this mode is different in the superfluid and normal phases of the photon gas due to the irrotational flow of a superfluid which does not allow for rigid-body rotation [69, 70]. At the moment we are trying to calculate if it is feasible to excite the photonic condensate to a scissor mode, such that one might experimentally prove the photonic condensate is a superfluid.

Additionally, we are investigating if the scissor mode is damped by the emission of condensate photons in pairs with opposite momentum. This would be a novel manifestation of the dynamical Casimir

[1] Private correspondence with J. Klaers and M. Weitz.

effect, which was first observed in 2011 in a very different system [71]. There are many questions worth investigating. Is the necessary frequency of oscillation of the mirrors feasible? Is the effect large enough to be experimentally observable? What is the spatial distribution of the photon emission from the condensate?

Note that in order to perform these experiments, one needs to have an anharmonic trapping frequency which can be tuned continuously. As we discussed in the previous section, this is not possible in the experimental setup used in Bonn: the trapping frequency is harmonic and can only be changed by using mirrors with a different radius of curvature and mirror separation. Therefore, it would be useful to use a different experimental setup and create a condensate of photons which is more flexible. In fact, a recently proposed idea for such a new type of experiment is to work with nano-fabricated semiconductor microcavities instead of dye-filled optical microcavities [70].

Appendix A

Detailed Calculations - Number Fluctuations

In this appendix we explicitly do calculations leading to some results we used in the chapter on number fluctuations.

A.1 Rate Equation Model

In this appendix we discuss a rate-equation model for the condensate of photons. Every process of absorption or emission depends on the number of photons n, the number of excited molecules $N_\uparrow$ and the number of ground-state molecules $N_\downarrow$. Therefore, the probability for every process is a function of all three: $p = p(n, N_\uparrow, N_\downarrow)$. A reasonable approximation is the Stosszahlansatz[1]: we assume that the probability factorizes as $p(n, N_\uparrow, N_\downarrow) = p_n p_{N_\uparrow} p_{N_\downarrow}$. Using this, we write down the master equation for the probability p_n to have n photons in the system

$$\frac{\mathrm{d}p_n}{\mathrm{d}t} = \sum_{N_\uparrow, N_\downarrow = 0}^{\infty} \Bigg[\Gamma \begin{pmatrix} n+1 \to n \\ N_\downarrow \to N_\downarrow - 1 \\ N_\uparrow \to N_\uparrow + 1 \end{pmatrix} p_{n+1} p_{N_\downarrow} p_{N_\uparrow} + \Gamma \begin{pmatrix} n-1 \to n \\ N_\downarrow \to N_\downarrow + 1 \\ N_\uparrow \to N_\uparrow - 1 \end{pmatrix} p_{n-1} p_{N_\downarrow} p_{N_\uparrow} - \Gamma \begin{pmatrix} n \to n-1 \\ N_\downarrow \to N_\downarrow - 1 \\ N_\uparrow \to N_\uparrow + 1 \end{pmatrix} p_n p_{N_\downarrow} p_{N_\uparrow} - \Gamma \begin{pmatrix} n \to n+1 \\ N_\downarrow \to N_\downarrow + 1 \\ N_\uparrow \to N_\uparrow - 1 \end{pmatrix} p_n p_{N_\downarrow} p_{N_\uparrow} \Bigg], \tag{A.1}$$

[1] This approximation was introduced for the first time by James Clerk Maxwell (1831 - 1879), who assumed that the velocities of colloiding particles are uncorrelated in the context of kinetic gas theory. He called this assumption *molecular chaos*. Ludwig Boltzmann (1844 - 1906) later refered to the approximation as the *Stosszahlansatz*, which translates as 'collision number hypothesis'.

where the first term and third term describe absorption and the second and fourth term emission of a photon. We integrated out the dependence on $N_\uparrow$ and $N_\downarrow$ by summing over all their possible values. The transition rates Γ can be calculated by using Fermi's golden rule. Generally, this amounts to evaluating matrix elements of the in and out state, which are of the typical form

$$\Gamma \begin{pmatrix} n \to n-1 \\ N_\downarrow \to N_\downarrow - 1 \\ N_\uparrow \to N_\uparrow + 1 \end{pmatrix} \propto |\langle N_\uparrow + 1, N_\downarrow - 1, n-1 | \hat{b}_\uparrow^\dagger \hat{b}_\downarrow \hat{a} | n, N_\downarrow, N_\uparrow \rangle|^2 = n(N_\uparrow + 1) N_\downarrow, \tag{A.2}$$

where $\hat{a}^\dagger$ ($\hat{a}$) represents the photon creation (annihilation operator, $\hat{b}^\dagger$ ($\hat{b}$) the molecular creation (annihilation) operator and we assumed the molecules to behave like bosons. In the end we shall take the classical limit for the molecules, such that the choice of describing the molecules by fermions or bosons should not matter. We proceed by setting the constant of proportionality in Eq. (A.2) to be A for an absorption process and E for an emission process. Performing the summations in Eq. (A.1), we obtain

$$\frac{\mathrm{d}p_n}{\mathrm{d}t} = A\langle N_\downarrow \rangle \langle N_\uparrow + 1 \rangle \left((n+1)p_{n+1} - np_n \right) + E\langle N_\uparrow \rangle \langle N_\downarrow + 1 \rangle \left(np_{n-1} - (n+1)p_n \right). \tag{A.3}$$

In order to obtain the time derivative of the average number of photons, we multiply Eq. (A.3) by n and sum over every possible amount of photons

$$\frac{\mathrm{d}\langle n \rangle}{\mathrm{d}t} \approx -A\langle n \rangle \langle N_\downarrow \rangle + E\langle n+1 \rangle \langle N_\uparrow \rangle, \tag{A.4}$$

where we took the classical limit for the molecules in the last step by setting $\langle N_{\downarrow/\uparrow} + 1 \rangle \approx 1$. Following exactly the same treatment, we find the time derivatives of the average number of ground-state and excited-state molecules

$$\begin{cases} \dfrac{\mathrm{d}\langle N_\uparrow \rangle}{\mathrm{d}t} \approx A\langle n \rangle \langle N_\downarrow \rangle - E\langle n+1 \rangle \langle N_\uparrow \rangle, \\ \dfrac{\mathrm{d}\langle N_\downarrow \rangle}{\mathrm{d}t} \approx -A\langle n \rangle \langle N_\downarrow \rangle + E\langle n+1 \rangle \langle N_\uparrow \rangle. \end{cases} \tag{A.5}$$

The time behavior of the whole system is now described by the two differential equations above and Eq. (A.3). In fact, by adding and substracting equations we see that the total number of molecules is constant: $\mathrm{d}\langle N \rangle / \mathrm{d}t = \mathrm{d}\langle N_\uparrow + N_\downarrow \rangle / \mathrm{d}t = 0$. Furthermore, we find that the sum of the average number of photons and excited molecules in the system is also constant: $\mathrm{d}\langle N_\uparrow + n \rangle / \mathrm{d}t = 0$. So we see that in our grand-canonical treatment we get the necessary conservation laws 'for free', although they are only valid on average. Now we proceed by assuming the detailed balance condition. In this system, it reads

$$\frac{E\langle N_\uparrow \rangle}{A\langle N_\downarrow \rangle} = e^{-\beta(\Delta - \Delta\mu)}, \tag{A.6}$$

with $\Delta\mu := \mu_\uparrow - \mu_\downarrow$ the difference in the chemical potentials of the excited-state and ground-state molecules and Δ the energy difference. If we consider the static case and substitute the detailed balance condition into Eq. (A.3) we find that

$$\langle n \rangle = \frac{1}{e^{\beta(\Delta - \Delta\mu)} - 1}, \tag{A.7}$$

i.e., the photons obey a Bose-Einstein distribution in equilibrium. This allows us to identify the chemical potential of photons μ to be in equilibrium equal to $\Delta\mu$.

A.2 Effective Action Thermal Lensing

Due to the fact that the action Eq. (3.16) contains both volume and surface integrals, it is easier to go to Fourier space. Thus, we define the necessary Fourier transforms as

$$\begin{cases} \phi(\mathbf{r},\tau) = (\hbar\beta V)^{-1/2} \sum_{\mathbf{p},n} a_{\mathbf{p},n} e^{i(\mathbf{p}\cdot\mathbf{r} - \omega_n \tau)}, \\ \phi_{\text{trans}}(\mathbf{x},\tau) = (\hbar\beta A)^{-1/2} \sum_{\mathbf{k},n} a_{\mathbf{k},n} e^{i(\mathbf{k}\cdot\mathbf{x} - \omega_n \tau)}, \\ \delta T(\mathbf{r},\tau) = (\hbar\beta V)^{-1/2} \sum_{\mathbf{p},n} \delta T_{\mathbf{p},n} e^{i(\mathbf{p}\cdot\mathbf{r} - \omega_n \tau)}, \end{cases} \tag{A.8}$$

with V the volume of the space, $A := V/D_0$ the corresponding area and $\omega_n = 2\pi n/\hbar\beta$ bosonic Matsubara frequencies. Note that we use the convention that a sum over $\mathbf{k}$ is over all vectors with a fixed z-component k_z and sums over $\mathbf{p}$ are ordinary three-dimensional sums. Substituting these Fourier transforms into the action Eq. (3.16), we arrive at

$$\begin{aligned} S[a, a^*, \delta T] = &\sum_{\mathbf{k},n} a^*_{\mathbf{k},n} (-\hbar G_\gamma^{-1}(\mathbf{k}, i\omega_n)) a_{\mathbf{k},n} + \sum_{\mathbf{p},n} \delta T^*_{\mathbf{p},n} (-\hbar G_T^{-1}(\mathbf{p}, i\omega_n)) \delta T_{\mathbf{p},n} \\ &+ \frac{1}{\sqrt{\hbar\beta V}} \left(\frac{mc^2\epsilon}{2n^2(T_0)} \right) \sum_{\mathbf{k},\mathbf{p},n,m} \left(a^*_{\mathbf{k}+\mathbf{p},m+n} a_{\mathbf{k},n} \delta T_{\mathbf{p},m} + a^*_{\mathbf{k},n} a_{\mathbf{k}+\mathbf{p},m+n} \delta T^*_{\mathbf{p},m} \right), \end{aligned} \tag{A.9}$$

where we used the fact that the temperature fluctuations are real-valued: $\delta T^*_{\mathbf{p},n} = \delta T_{-\mathbf{p},-n}$. In the process we defined the inverse propagator in Fourier space for the temperature fluctuations

$$-\hbar G_T^{-1}(\mathbf{p}, \omega_n) = \frac{1}{T_0} \left(c_p - \frac{\kappa |\mathbf{p}|^2}{\omega_n} \right). \tag{A.10}$$

The partition function corresponding to the theory described by the action Eq. (A.9) is given by a path integral as

$$Z = \int \mathrm{d}[a^*]\, \mathrm{d}[a]\, \mathrm{d}[\delta T] \exp\left(-\frac{S[a, a^*, \delta T]}{\hbar} \right). \tag{A.11}$$

Hence, we complete the square for the field $\delta T_{\mathbf{p},n}$ in Eq. (A.9), perform the associated path integral over $\delta T_{\mathbf{p},n}$ and re-exponentiate to arrive at

$$Z = \int \mathrm{d}[a^*]\,\mathrm{d}[a] \exp\left(-\frac{S^{\mathsf{eff}}[a,a^*]}{\hbar}\right) \tag{A.12}$$

with the effective action

$$\begin{aligned} S^{\mathsf{eff}}[a,a^*] =& \sum_{\mathbf{k},n} a^*_{\mathbf{k},n}(-\hbar G_\gamma^{-1}(\mathbf{k}, i\omega_n))a_{\mathbf{k},n} - \hbar \mathsf{Tr}[\log(-G_T^{-1}(\mathbf{p},\omega_n))] \\ & -\frac{1}{\hbar^2 \beta V}\left(\frac{mc^2\epsilon}{2n^2(T_0)}\right)^2 \sum_{\substack{\mathbf{k},\mathbf{p},\mathbf{k}' \\ n,m,n'}} G_T(\mathbf{p},\omega_m) a^*_{\mathbf{k}+\mathbf{p},n+m} a_{\mathbf{k},n} a^*_{\mathbf{k}',n'} a_{\mathbf{k}'+\mathbf{p},n'+m}, \end{aligned} \tag{A.13}$$

Note that the emergence of the second term in the expression above is the result from the path integral over $\delta T_{\mathbf{p},n}$, whereas the last term comes from completing the square. It is this last term which gives an effective photon-photon interaction, mediated by the temperature fluctuation.

A.3 Effective Action Dye-Mediated Photon-Photon Scattering

By using the action in Eq. (4.11), we write down the partition function Z of the theory as a path integral over the photonic and molecular fields. We denote the photonic part of the action Eq. (4.11) by S_γ, the molecular part by S_0 and the interaction part by S_{int}. Subsequently, we perform perturbation theory in the interaction parameter g_{mol} to integrate out the molecules [36], i.e.,

$$\begin{aligned} Z &= \int \mathrm{d}[a^*]\,\mathrm{d}[a]\,\mathrm{d}[b^*_\downarrow]\,\mathrm{d}[b_\downarrow]\,\mathrm{d}[b^*_\uparrow]\,\mathrm{d}[b_\uparrow] \exp\left(-\frac{1}{\hbar}\left(S_\gamma + S_0 + S_{\mathsf{int}}\right)\right) \\ &= Z_0 \int \mathrm{d}[a^*]\,\mathrm{d}[a] \exp\left(-\frac{1}{\hbar}S_\gamma\right)\left(1 + \frac{1}{2\hbar^2}\langle S^2_{\mathsf{int}}\rangle_0 + \frac{1}{24\hbar^4}\langle S^4_{\mathsf{int}}\rangle_0 + \mathcal{O}(g^6_{\mathsf{mol}})\right), \end{aligned} \tag{A.14}$$

where we used the fact that $\langle S^m_{\mathsf{int}}\rangle_0 = 0$ if m is odd and defined

$$\begin{cases} Z_0 := \int \mathrm{d}[b^*_\downarrow]\,\mathrm{d}[b_\downarrow]\,\mathrm{d}[b^*_\uparrow]\,\mathrm{d}[b_\uparrow] \exp(-S_0/\hbar), \\ \langle \dots \rangle_0 := \dfrac{1}{Z_0}\displaystyle\int \mathrm{d}[b^*_\downarrow]\,\mathrm{d}[b_\downarrow]\,\mathrm{d}[b^*_\uparrow]\,\mathrm{d}[b_\uparrow](\dots)\exp(-S_0/\hbar). \end{cases} \tag{A.15}$$

By using Wick's theorem we find for the term at order g^2_{mol}

$$\langle S^2_{\mathsf{int}}\rangle_0 = -\frac{2g^2_{\mathsf{mol}}}{\hbar\beta V}\sum_{\mathbf{k},\mathbf{p},n,n'} a^*_{\mathbf{k},n} a_{\mathbf{k},n} G_\uparrow(\mathbf{p}+\mathbf{k}, i(\omega_n + \omega_{n'}))G_\downarrow(\mathbf{p}, i\omega_{n'}). \tag{A.16}$$

This term can be interpreted as a self-energy for the photons. We do a similar computation for the term at order g^4_{mol}. Expanding out the interaction term yields sixteen terms, of which ten do not contain the appropriate combination of fields to yield a non-zero result when we Wick contract them. The remaining six terms turn out to be identical, yielding

$$\begin{aligned}\langle S^4_{\mathsf{int}}\rangle_0 = \frac{12 g^4_{\mathsf{mol}}}{(\hbar\beta V)^2} \sum_{\substack{\mathbf{p},\mathbf{k},\mathbf{k}',\mathbf{k}'' \\ n,n',n'',m}} a^*_{\mathbf{k},n} a_{\mathbf{k}',n'} a^*_{\mathbf{k}'',n''} a_{\mathbf{k}-\mathbf{k}'+\mathbf{k}'',n-n'+n''} \Big[G_\uparrow(\mathbf{p}+\mathbf{k}, i(\omega_m+\omega_n)) \\ \times G_\downarrow(\mathbf{p}, i\omega_m) G_\uparrow(\mathbf{p}+\mathbf{k}', i(\omega_m+\omega_{n'})) G_\downarrow(\mathbf{p}+\mathbf{k}'-\mathbf{k}'', i(\omega_m+\omega_{n'}-\omega_{n''})) \Big] \\ - \frac{12 g^4_{\mathsf{mol}}}{(\hbar\beta V)^2} \Big(\sum_{\mathbf{p},\mathbf{k},n,n'} a^*_{\mathbf{k},n} a_{\mathbf{k},n} G_\uparrow(\mathbf{p}+\mathbf{k}, i(\omega_n+\omega_{n'})) G_\downarrow(\mathbf{p}, i\omega_n) \Big)^2 . \end{aligned} \tag{A.17}$$

The first term can be diagrammatically displayed as a box diagram. The second term can be represented by a disconnected diagram: it is simply one half times the square of the self-energy diagram. All disconnected diagrams disappear automatically when we sum the connected diagrams into an exponent. Hence, the sum of the self-energy and the box diagram gives us the desired effective action

$$\begin{aligned} S^{\mathsf{eff}}[a^*, a] = \sum_{\mathbf{k},n} a^*_{\mathbf{k},n} \Big(-i\hbar\omega_n + \epsilon_\gamma(\mathbf{k}) - \mu + \hbar\Sigma(\mathbf{k}, i\omega_n) \Big) a_{\mathbf{k},n} \\ + \frac{1}{2\hbar\beta V} \sum_{\substack{\mathbf{k},\mathbf{k}',\mathbf{k}'' \\ n,n',n''}} \Gamma^{(4)}(\mathbf{k},\mathbf{k}',\mathbf{k}'', i\omega_n, i\omega_{n'}, i\omega_{n''}) a^*_{\mathbf{k},n} a_{\mathbf{k}',n'} a^*_{\mathbf{k}'',n''} a_{\mathbf{k}-\mathbf{k}'+\mathbf{k}'',n-n'+n''}, \end{aligned} \tag{A.18}$$

where the photon self-energy and the photon-photon scattering vertex are defined as in Eqs. (3.24) and (3.25).

A.4 Calculation Imaginary Part Self-Energy Photons

By using Fermi's golden rule we calculate the absorption cross section from the imaginary part of the self-energy given by Eq. (3.24). To avoid divergencies when calculating the photon-photon interaction we first introduce a finite lifetime for the excited molecular state. To do this we recall that the spectral function $\rho(\mathbf{k}, \omega)$ is defined as

$$\rho(\mathbf{k}, \omega) := -\frac{1}{\pi\hbar} \mathsf{Im} \left[G^{(+)}(\mathbf{k}, \omega) \right], \tag{A.19}$$

where the retarded Green's function follows from a Wick rotation of the Green's function: $G^{(+)}(\mathbf{k}, \omega) = G(\mathbf{k}, i\omega_n \to \omega + i0)$. Given a spectral function, we calculate the corresponding Green's function by using the following relation

$$G_\uparrow(\mathbf{k}, i\omega_n) = \hbar \int_{-\infty}^{\infty} \mathrm{d}\omega \frac{\rho_\uparrow(\mathbf{k}, \omega)}{i\omega_n - \omega}. \tag{A.20}$$

For a free theory the spectral function is just a delta function centered around the single-particle energy. We give the excited molecule a finite lifetime by broadening the spectral function to a Gaussian profile, i.e.,

$$\rho_\uparrow(\mathbf{k},\omega) = \frac{1}{\sqrt{2\pi}\hbar\Gamma}\exp\left(-\frac{(\hbar\omega-\epsilon(\mathbf{k})-\Delta+\mu_\uparrow)^2}{2(\hbar\Gamma)^2}\right), \tag{A.21}$$

such that the spectral function satisfies the frequency sum rule $\int_{-\infty}^{\infty}\mathrm{d}\hbar\omega\rho_\uparrow(\mathbf{k},\omega)=1$. Note that this spectral function is still centered around the single-particle energy of the excited molecule and that we have

$$\lim_{\Gamma\to 0}\rho_\uparrow(\mathbf{k},\omega) = \delta(\hbar\omega-\epsilon(\mathbf{k})-\Delta+\mu_\uparrow). \tag{A.22}$$

We consider the molecules in the classical limit. Thus, by using the Maxwell-Boltzmann distribution $N_{\mathsf{MB}}(x) := \exp(-\beta x)$, the molecule density in the excited state $n_\uparrow$ is equal to

$$\begin{aligned} n_\uparrow &\approx \frac{1}{V}\int_{-\infty}^{\infty}\mathrm{d}\hbar\omega\sum_{\mathbf{k}}\rho_\uparrow(\mathbf{k},\omega)N_{\mathsf{MB}}(\hbar\omega) \\ &= \frac{1}{\Lambda^3}\exp\left(\beta\mu_\uparrow-\beta\Delta+\frac{1}{2}(\beta\hbar\Gamma)^2\right), \end{aligned} \tag{A.23}$$

where the thermal de Broglie wavelength Λ is defined as $\Lambda := \sqrt{2\pi\beta\hbar^2/M}$. As $\lim_{\omega\to-\infty}N_{\mathsf{FD}}(\omega)=1$ and we integrate over ω, the approximation in the calculation above is only valid when the spectral function is almost zero for negative ω. As the spectral function is centered around $\hbar\omega=\epsilon(\mathbf{k})+\Delta-\mu_\uparrow$, a reasonable restriction is $\Delta-\mu_\uparrow-2\Gamma\hbar>0$. This condition is fulfilled for the values of Δ and Γ we use. We are thus allowed to take the limit $N_{\mathsf{FD}}(\omega)\to N_{\mathsf{MB}}(\omega)$ in the following, even if we integrate over ω.

Note that in the ground state the molecules still have an infinite lifetime and therefore the density of molecules in the ground state is given by $n_\downarrow = \Lambda^{-3}\exp\left(\beta\mu_\downarrow\right)$. We express the chemical potential of the ground state in terms of $\Delta\mu := \mu_\uparrow-\mu_\downarrow$ and $n_{\mathsf{mol}} := n_\downarrow+n_\uparrow$ as

$$\exp\left(\beta\mu_\downarrow\right) = \frac{n_{\mathsf{mol}}\Lambda^3}{1+\exp\left(\beta(\Delta\mu-\Delta)+(\hbar\beta\Gamma)^2/2\right)}, \tag{A.24}$$

which is a relation we will use later on. We now explicitly calculate the self-energy by starting from the definition provided in Eq. (3.24) and invoking Eqs. (A.20) and (A.21)

$$\begin{aligned} \hbar\Sigma(\mathbf{k},i\omega_n) &= \frac{g_{\mathsf{mol}}^2}{\hbar^2\beta V}\sum_{\mathbf{p},m}G_\downarrow(\mathbf{p},i\omega_m)G_\uparrow(\mathbf{p}+\mathbf{k},i(\omega_m+\omega_n)) \\ &= \frac{g_{\mathsf{mol}}^2}{\hbar\beta V}\sum_{\mathbf{p},m}\int_{-\infty}^{\infty}\mathrm{d}\hbar\omega'\left(\frac{\rho_\uparrow(\mathbf{p}+\mathbf{k},\omega')}{i\hbar(\omega_n+\omega_m)-\hbar\omega'}\right)\left(\frac{-\hbar}{-i\hbar\omega_m+\epsilon(\mathbf{p})-\mu_\downarrow}\right) \\ &= \frac{g_{\mathsf{mol}}^2}{V}\sum_{\mathbf{p}}\int_{-\infty}^{\infty}\mathrm{d}\hbar\omega'\left(\frac{\rho_\uparrow(\mathbf{p}+\mathbf{k},\omega')}{-i\hbar\omega_n+\hbar\omega'-\epsilon(\mathbf{p})+\mu_\downarrow}\right)\Big(N_{\mathsf{FD}}(\hbar\omega')-N_{\mathsf{FD}}(\epsilon(\mathbf{p})-\mu_\downarrow)\Big), \end{aligned} \tag{A.25}$$

where we performed the Matsubara summation and introduced the Fermi-Dirac distribution, which is defined as $N_{\mathsf{FD}}(x) := (\exp(\beta x)+1)^{-1}$. Since we are considering a bath of molecules at room temperature, we are allowed to take the limit $N_{\mathsf{FD}}(x) \to N_{\mathsf{MB}}(x) := \exp(-\beta x)$. Furthermore, we perform a Wick rotation to obtain the retarded self-energy. The only term that changes in the self-energy is

$$\frac{1}{-i\hbar\omega_n - \epsilon(\mathbf{p}) + \mu_\downarrow + \hbar\omega'} \to i\pi\delta(\hbar\omega' - \epsilon(\mathbf{p}) + \mu_\downarrow - \hbar\omega) + \mathcal{P}\left(\frac{1}{\hbar\omega' - \epsilon(\mathbf{p}) + \mu_\downarrow - \hbar\omega}\right), \quad \text{(A.26)}$$

with the symbol $\mathcal{P}$ symbolizing the principal value of the fraction. With the help of the relationships above, we find for the imaginary part of the self-energy

$$\begin{aligned} R(\mathbf{k}_+,\omega) &:= -\mathrm{Im}(\hbar\Sigma^{(+)}(\mathbf{k}_+,\omega)) \\ &= -\frac{\pi g_{\mathsf{mol}}^2}{V}\sum_{\mathbf{p}}\int_{-\infty}^{\infty}\mathrm{d}\hbar\omega'\rho_\uparrow(\mathbf{p}+\mathbf{k}_+,\omega')\delta(\hbar\omega'-\epsilon(\mathbf{p})+\mu_\downarrow-\hbar\omega)\left(e^{-\beta\hbar\omega'}-e^{-\beta(\epsilon(\mathbf{p})-\mu_\downarrow)}\right) \\ &= \frac{\sqrt{\pi}g_{\mathsf{mol}}^2\beta\,\exp\left(\beta\mu_\downarrow\right)\left(1-\exp\left(-\beta\hbar\omega\right)\right)}{\Lambda^3\sqrt{2(2\beta\epsilon(\mathbf{k}_+)+(\hbar\beta\Gamma)^2)}}\,\exp\left(\frac{-(\epsilon(\mathbf{k}_+)+\Delta-\Delta\mu-\hbar\omega)^2}{2((\hbar\Gamma)^2+2\epsilon(\mathbf{k}_+))}\right), \end{aligned} \quad \text{(A.27)}$$

with $\mathbf{k}_+ = (0,0,k_z)$ the wave number for photons in the condensate. By setting $\Delta\mu = 0$ and $k_z = \omega/c$ and taking the part of the expression above proportional to $N_\downarrow$, we obtain the absorption cross section at equilibrium. As it turns out the result is almost (or in very good approximation) independent of the exact value k_z, and therefore from now onwards we take $k_z = 0$, thereby simplifying our treatment considerably. Using Fermi's Golden rule in the form $\sigma_{\mathsf{abs}}(\omega) = 2R_{\mathsf{abs}}(\omega)/c\hbar N_\downarrow$, we we find

$$\sigma_{\mathsf{abs}}(\omega)\big|_{k_z=0} = \frac{\sqrt{2\pi}g_{\mathsf{mol}}^2}{\hbar^2\Gamma c}\exp\left(-\frac{(\hbar\omega-\Delta)^2}{2\hbar^2\Gamma^2}\right). \quad \text{(A.28)}$$

A.5 Calculation Box-Diagram

We now evaluate the photon-photon interacting strength in the condensate, i.e., with Matsubara frequency zero, and set $k_z = 0$, as is justified by the previous section. This amounts to the Feynman diagram in Fig. A.1. By using $G_\downarrow^2(\mathbf{p},m) = -\hbar\partial_\downarrow G_\downarrow(\mathbf{p},m)$, we obtain

$$\begin{aligned} \Gamma^{(4)}(\mathbf{0},\mathbf{0},\mathbf{0},0,0,0) &= \frac{g_{\mathsf{mol}}^4}{\hbar^3\beta V}\partial_\downarrow\sum_{\mathbf{p},m}G_\uparrow^2(\mathbf{p},m)G_\downarrow(\mathbf{p},m) \\ &= \frac{g_{\mathsf{mol}}^4\partial_\downarrow}{2\pi\beta\hbar^4\Gamma^2\Lambda^3}\int_{-\infty}^{\infty}\mathrm{d}\hbar\omega\int_{-\infty}^{\infty}\mathrm{d}\hbar\omega'\exp\left(\beta\mu_\downarrow-\frac{(\hbar\omega+\Delta\mu-\Delta)^2)+(\hbar\omega'+\Delta\mu-\Delta)^2}{2(\hbar\Gamma)^2}\right) \\ &\qquad\times\frac{1}{\omega-\omega'}\left(\frac{1}{\omega'}(1-e^{-\beta\hbar\omega'})-\frac{1}{\omega}(1-e^{-\beta\hbar\omega})\right) \end{aligned} \quad \text{(A.29)}$$

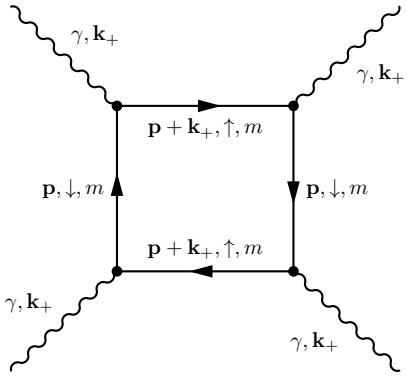

Figure A.1: Feynman diagram for a fourth-order photon-photon interaction. The photons γ are considered to be part of the condensate and are thus at zero frequency and momentum $\mathbf{k}_+ = (0, 0, k_z)$, as their z-component momentum is fixed and $k_x = k_y = 0$ for the ground state of the homogeneous photon gas. The molecule forms a closed loop of ground ($\downarrow$) and excited ($\uparrow$) states, with momentum $\mathbf{p}$ and Matsubara frequency ω_m.

where we again performed the Matsubara summation, we took the limit $N_{\mathsf{FD}}(x) \to N_{\mathsf{MB}}(x)$ and finally performed the $\mathbf{p}$-integral. After we have substituted Eq. (A.24), we perform the differentiation. Setting $\Delta\mu - \Delta := \mu - \delta$ and introducing the dimensionless quantities $\omega := \beta\hbar\omega$, $\omega' := \beta\hbar\omega'$, we obtain

$$\begin{aligned}\Gamma^{(4)}(\mathbf{0},\mathbf{0},\mathbf{0},0,0,0) = \frac{g_{\mathsf{mol}}^4 \beta n_{\mathsf{mol}}}{2\pi\hbar^2\Gamma^2\{1+\exp\left(\beta\mu-\beta\delta+(\beta\hbar\Gamma)^2/2\right)\}} \int_{-\infty}^{\infty} \mathrm{d}\omega \int_{-\infty}^{\infty} \mathrm{d}\omega' (\omega-\omega')^{-1} \\ \times \exp\left(-\frac{(\omega+\beta\mu-\beta\delta)^2+(\omega'+\beta\mu-\beta\delta)^2}{2(\beta\hbar\Gamma)^2}\right) \\ \times \left(\frac{1}{\omega'}(1-e^{-\omega'})-\frac{1}{\omega}(1-e^{-\omega})\right)\left(1+\frac{\omega+\omega'+2\beta(\mu-\delta)}{(\beta\hbar\Gamma)^2}\right) \\ := \frac{g_{\mathsf{mol}}^4 \beta n_{\mathsf{mol}}}{\hbar^2\Gamma^2} f(\beta\mu-\beta\delta), \end{aligned} \tag{A.30}$$

with $f(\beta\mu - \beta\delta)$ a smooth dimensionless function peaked around zero. Again we must scale $\Gamma^{(4)} \to 2\Gamma^{(4)}/3D_0$, as the photon gas is confined to two dimensions, to obtain the effective coupling constant g of the photons in the condensate.

Appendix B

Detailed Calculations - Phase Diffusion

In this appendix we explicitly do calculations leading to some results we used in the chapter on phase diffusion.

B.1 General solution Schrödinger equation phase

In this section we solve the Schrödinger equation for the phase as it is given in Eq. (4.15) by

$$i\hbar\frac{\partial\Psi(\theta,t)}{\partial t} = -\frac{g}{2A_{\mathsf{TF}}}\left(\frac{\partial}{\partial\theta} + iN_0\right)^2\Psi(\theta,t). \tag{B.1}$$

We invoke separation of variables in the form of the ansatz $\Psi(\theta_0,t) = T(t)\Theta(\theta_0)$. Substituting this in the differential equation yields

$$\frac{i\hbar}{T(t)}\frac{\mathrm{d}T(t)}{\mathrm{d}t} = -D\bigg(-N_0^2 + \frac{2iN_0}{\Theta(\theta)}\frac{\mathrm{d}\Theta(\theta)}{\mathrm{d}\theta} + \frac{1}{\Theta(\theta)}\frac{\mathrm{d}^2\Theta(\theta)}{\mathrm{d}\theta^2}\bigg), \tag{B.2}$$

such that we may conclude that both sides of the equality should equal the same constant, which we call E. The time-dependent part is given by

$$\frac{\mathrm{d}T(t)}{\mathrm{d}t} = \frac{E}{i\hbar}T(t), \tag{B.3}$$

which is solved by $T(t) \propto e^{-iEt/\hbar}$. For the phase-dependent part we find

$$\frac{\mathrm{d}^2\Theta(\theta)}{\mathrm{d}\theta^2} + 2iN_0\frac{\mathrm{d}\Theta(\theta)}{\mathrm{d}\theta} + \left(\frac{E}{D} - N_0^2\right)\Theta(\theta) = 0. \tag{B.4}$$

In order to solve this ordinary differential equation, we make an additional ansatz of the form $\Theta(\theta) \propto e^{\lambda\theta}$. Substitution yields a characteristic equation with solutions $\lambda_\pm = -i(N_0 \pm \sqrt{E/D})$. Thus, the full wave function becomes

$$\Psi(\theta, t) = \left(\alpha e^{i\theta\sqrt{E/D}} + \beta e^{-i\theta\sqrt{E/D}}\right) e^{-i(Et/\hbar + N_0\theta)}, \tag{B.5}$$

where $\alpha, \beta \in \mathbb{C}$ are integration constants. By demanding periodicity, i.e., $\Psi(\theta, t) = \Psi(\theta + 2\pi, t)$, we find

$$\alpha + \beta = \alpha e^{2\pi i\sqrt{E/D}} + \beta e^{-2\pi i\sqrt{E/D}}, \tag{B.6}$$

which yields a quantized energy $E_n = D(n + N_0)^2$, for $n \in \mathbb{Z}$. The general solution now becomes

$$\Psi(\theta, t) = \sum_{n\in\mathbb{Z}} c_n \exp\left(-\frac{iD(n + N_0)^2 t}{\hbar} + in\theta\right). \tag{B.7}$$

The constants c_n can be found when an initial wavefunction $\Psi(\theta, 0)$ is provided. In the next section we do this calculation for a Gaussian initial wavefunction.

B.2 Specific Solution Schrödinger Equation Phase

We start with an unnormalized initial wavefunction which is a superposition of Gaussians centered around $\theta = 0 \bmod 2\pi$,

$$\Psi(\theta, 0) = \alpha \sum_{n\in\mathbb{Z}} e^{-(\theta+2\pi n)^2/2\sigma^2}. \tag{B.8}$$

Note that this wavefunction is constructed such that is periodic in θ. The normalization of the wavefunction determines the value of α. Thus,

$$\begin{aligned}
\int_0^{2\pi} \mathrm{d}\theta\ |\Psi(\theta, 0)|^2 &= |\alpha|^2 \sum_{n,m\in\mathbb{Z}} \int_0^{2\pi} \mathrm{d}\theta\ e^{-(\theta+2\pi n)^2/2\sigma^2} e^{-(\theta+2\pi m)^2/2\sigma^2} \\
&= |\alpha|^2 \sum_{n,m\in\mathbb{Z}} \int_{2\pi n}^{2\pi(n+1)} \mathrm{d}\theta\ e^{-\theta^2/2\sigma^2} e^{-(\theta+2\pi(m-n))^2/2\sigma^2} \\
&= |\alpha|^2 \sum_{m\in\mathbb{Z}} e^{-(\pi m)^2/\sigma^2} \int_{-\infty}^{\infty} \mathrm{d}\theta\ e^{-(\theta+\pi m)^2/\sigma^2} \\
&= |\alpha|^2 \sqrt{\pi}\sigma \sum_{m\in\mathbb{Z}} e^{-(\pi m)^2/\sigma^2}.
\end{aligned} \tag{B.9}$$

In general we are interested in sharply-peaked wavefunctions, where the phase of the Bose-Einstein condensate is well-defined. In this case $\sigma \ll 1$ and we have in very good approximation

$$\alpha = \frac{1}{(\pi\sigma^2)^{1/4}}\left(\sum_{m\in\mathbb{Z}} e^{-(\pi m)^2/\sigma^2}\right)^{-1} \approx \frac{1}{(\pi\sigma^2)^{1/4}}. \tag{B.10}$$

The coefficients c_n can be determined by using the orthogonality of the basis $\{e^{in\theta}\}_{n\in\mathbb{Z}}$. We find

$$\begin{aligned} c_n &= \frac{1}{2\pi}\int_0^{2\pi} \mathrm{d}\theta\ \Psi(\theta,0)e^{-in\theta} \\ &= \frac{\alpha}{2\pi}\int_0^{2\pi} \mathrm{d}\theta\ \sum_{m\in\mathbb{Z}} e^{-(\theta+2\pi m)^2/2\sigma^2}e^{-in\theta} \\ &= \frac{\alpha}{2\pi}\int_{-\infty}^{\infty} \mathrm{d}\theta\ e^{-\theta^2/2\sigma^2}e^{-in\theta} \\ &= \frac{\alpha\sigma}{\sqrt{2\pi}}e^{-n^2\sigma^2/2} \approx \left(\frac{\sigma^2}{4\pi^3}\right)^{1/4} e^{-n^2\sigma^2/2}, \end{aligned} \tag{B.11}$$

where we used the approximate value for α from Eq. (B.10). Hence we find for the total wavefunction

$$\Psi(\theta,t) = \left(\frac{\sigma^2}{4\pi^3}\right)^{1/4} \sum_{n\in\mathbb{Z}} \exp\left(-\frac{iD(n+N_0)^2t}{\hbar} + in\theta - \frac{n^2\sigma^2}{2}\right). \tag{B.12}$$

B.3 Interference due to Quantum Fluctuations

By using the wavefunction we calculated in the previous section, the interference pattern due to quantum fluctuations can now be calculated explicitly,

$$\begin{aligned} \bar{I}_I(\mathbf{r},t) &:= 2A_I(\mathbf{r},t)\int_0^{2\pi} \mathrm{d}\theta |\Psi(\theta,t)|^2\cos\theta \\ &= \frac{A_I(\mathbf{r},t)\sigma}{\pi^{3/2}} \sum_{m,n\in\mathbb{Z}} \exp\left[\frac{iDt}{\hbar}\Big((m+N_0)^2 - (n+N_0)^2\Big) - \frac{\sigma^2(m^2+n^2)}{2}\right] \\ &\qquad \times \int_0^{2\pi} \mathrm{d}\theta e^{i(n-m)\theta}\cos\theta, \end{aligned} \tag{B.13}$$

The integral on the second line yields

$$\int_0^{2\pi} \mathrm{d}\theta \exp(i(n-m)\theta)\cos\theta = 2\pi(\delta_{n,m-1} + \delta_{n,m+1}). \tag{B.14}$$

Substituting this expression into $\bar{I}_I$, we obtain

$$\begin{aligned}\bar{I}_I(\mathbf{r},t) &= \frac{2A_I(\mathbf{r},t)\sigma}{\sqrt{\pi}}\sum_{n\in\mathbb{Z}}\Bigg\{\exp\left[i\frac{Dt}{\hbar}\Big((n+1+N_0)^2-(n+N_0)^2\Big)-\frac{\sigma^2((n+1)^2+n^2)}{2}\right]\\ &\qquad+\exp\left[i\frac{Dt}{\hbar}\Big((n-1+N_0)^2-(n+N_0)^2\Big)-\frac{\sigma^2((n-1)^2+n^2)}{2}\right]\Bigg\}\\ &= \frac{4A_I(\mathbf{r},t)\sigma}{\sqrt{\pi}}e^{-\sigma^2/2}\sum_{n\in\mathbb{Z}}e^{-n(n+1)\sigma^2}\cos\left(\frac{(2n+1+2N_0)Dt}{\hbar}\right),\end{aligned} \tag{B.15}$$

where we used Euler's formula to write the complex exponential in terms of a cosine and a sine. After a shift in the sums, the imaginary parts cancelled and the real parts added up. For small σ and the assumption $N_0 \gg 1$ (which is compatible with the fact that we used the Thomas-Fermi limit when we derived the Schrödinger equation for the phase) this reduces to

$$\bar{I}_{\mathrm{I}}(\mathbf{r},t) \approx \frac{4A_{\mathrm{I}}(\mathbf{r},t)\sigma}{\sqrt{\pi}}\cos\left(\frac{5(1+2N_0)\sigma t}{2t_{\mathrm{col}}}\right)\sum_{n\in\mathbb{Z}}\cos\left(\frac{5n\sigma t}{t_{\mathrm{col}}}\right)e^{-n(n+1)\sigma^2}, \tag{B.16}$$

where we introduced the characteristic time scale $t_{\mathsf{col}} = 5\hbar\sigma/2D$. The result in Eq. (B.16) can be simplified by noting that for small σ we can approximate the envelop function by

$$\begin{aligned}\sigma\sum_{n\in\mathbb{Z}}e^{-\sigma^2 n(n+1)}\cos\left(\frac{5n\sigma t}{t_{\mathsf{col}}}\right) &\approx \sigma\sum_{n\in\mathbb{Z}}e^{-\sigma^2 n^2}\cos\left(\frac{5n\sigma t}{t_{\mathsf{col}}}\right)\\ &\approx \int_{-\infty}^{\infty}\mathrm{d}x\; e^{-x^2}\cos\left(\frac{5xt}{t_{\mathsf{col}}}\right)\\ &= \sqrt{\pi}\mathsf{exp}\left(-\frac{25t^2}{t_{\mathsf{col}}^2}\right).\end{aligned} \tag{B.17}$$

Thus, we find in total for the interence pattern

$$\bar{I}_{\mathrm{I}}(\mathbf{r},t) \approx 4A_I(\mathbf{r},t)\cos\left(\frac{5(1+2N_0)\sigma t}{2t_{\mathsf{col}}}\right)\mathsf{exp}\left(-\frac{25t^2}{t_{\mathsf{col}}^2}\right). \tag{B.18}$$

Bibliography

[1] S. Bose, *Plancks Law and Light Quantum Hypothesis*, Z. Phys. **26**, 178 (1924).

[2] A. Einstein, *Quantentheorie des einatomigen idealen Gases*, Sitz. ber. Preuss. Akad. Wiss. **1**, 3 (1925).

[3] M.H. Anderson, J.R. Ensher, M.R. Matthews, C.E. Wieman, E.A. Cornell, *Observation of Bose-Einstein Condensation in a Dilute Atomic Vapor*, Science **269**, 5221 (1995).

[4] C.C. Bradley, C.A. Sackett, J.J. Tollett and R.G. Hulet, *Evidence of Bose-Einstein Condensation in an Atomic Gas with Attractive Interactions*, Phys. Rev. Lett. **75**, 1687 (1995).

[5] K.B. Davis, M.O. Mewes, M.R. Andrews, N.J. van Druten, D.S. Durfee, D.M. Kurn and W. Ketterle, *Bose-Einstein Condensation in a Gas of Sodium Atoms*, Phys. Rev. Lett. **75**, 3969 (1995).

[6] J. Kasprzak, M. Richard, S. Kundermann, A. Baas, P. Jeambrun, J.M.J. Keeling, F.M. Marchetti, M.H. Szymańska, R. Andr, J.L. Staehli, V. Savona, P.B. Littlewood, B. Deveaud and Le Si Dang, *Bose-Einstein condensation of Exciton Polaritons*, Nature **443**, 409 (2006).

[7] R. Balili, V. Hartwell, D. Snoke1, L. Pfeiffer and K. West, *Bose-Einstein Condensation of Microcavity Polaritons in a Trap*, Science **316**, 1007 (2007).

[8] S.O. Demokritov, V.E. Demidov, O. Dzyapko, G.A. Melkov, A.A. Serga, B. Hillebrands and A.N. Slavin, *Bose-Einstein Condensation of Quasi-Equilibrium Magnons at Room Temperature under Pumping*, Nature **443**, 430 (2006).

[9] J. Klaers, J. Schmitt, F. Vewinger and M. Weitz, *Bose-Einstein Condensation of Photons in an Optical Microcavity*, Nature **468**, 545 (2010).

[10] J. Schmitt, T. Damm, D. Dung, F. Vewinger, J. Klaers and M. Weitz, *Observation of Grand-Canonical Number Statistics in a Photon Bose-Einstein Condensate*, Phys. Rev. Lett. **112**, 030401 (2014).

[11] K. Huang, *Statistical Mechanics*, Wiley (1987).

[12] Y.B. Zel'dovich and E.V. Levich, *Bose Condensation and Shock Waves in Photon Spectra*, Sov. Phys. JETP **28**, 1287 (1969).

[13] R.Y. Chiao and J. Boyce, *Bogoliubov dispersion relation and the possibility of superfluidity for weakly interacting photons in a two-dimensional photon fluid*, Phys. Rev. A **60**, 4114 (1999).

[14] R.Y. Chiao, *Bogoliubov dispersion relation for a 'photon fluid': Is this a superfluid?*, Optics Communications **179**, 157 (2000).

[15] M.W. Mitchell, C.I. Hancox, R.Y. Chiao, *Dynamics of atom-mediated photon-photon scattering*, Phys. Rev. A **62**, 043819 (2000).

[16] E.L. Bolda, R.Y. Chiao and W.H. Zurek, *Dissipative Optical Flow in a Nonlinear Fabry-Pérot Cavity*, Phys. Rev. Lett. **86**, 416 (2001).

[17] J. Klaers, F. Vewinger and M. Weitz, *Thermalization of a two-dimensional photonic gas in a 'white wall' photon box*, Nature Physics **6**, 512 (2010).

[18] J. Klaers, J. Schmitt, T. Damm, F. Vewinger and M. Weitz, *Bose-Einstein condensation of paraxial light*, Appl. Phys. B **105**, 17 (2011).

[19] J. Klaers and M. Weitz, *Bose-Einstein condensation of photons*, arXiv:1210.7707 [quant-ph] (2012).

[20] J. Klaers, J. Schmitt, T. Damm, F. Vewinger and M. Weitz, *Statistical Physics of Bose-Einstein-Condensed Light in a Dye Microcavity*, Phys. Rev. Lett. **108**, 160403 (2012).

[21] C.C. Gerry and P.L. Knight, *Introductory Quantum Optics*, Cambridge University Press (2005).

[22] J. Klaers, *Bose-Einstein-Kondensation von paraxialem Licht*, PhD thesis, University of Bonn (2010).

[23] Jan Klaers, Julian Schmitt, Tobias Damm, David Dung, Frank Vewinger and Martin Weitz, *Bose-Einstein Condensation of Photons in a Microscopic Optical Resonator: Towards Photonic Lattices and Coupled Cavities*, Proc. SPIE 8600, 86000L (2013).

[24] H. Smith and C.J. Pethick, *Bose-Einstein Condensation in Dilute Gases*, Cambridge University Press, 2nd Edition (2008).

[25] C. Beenakker and C. Schönenberger, *Quantum shot noise*, Physics Today **56**, 37 (2003).

[26] W. Schottky, *Über spontane Stromschwankungen in verschiedenen Elektrizitätsleitern*, Ann. Phys. **57**, 541 (1918).

[27] F. Lefloch, C. Hoffmann, M. Sanquer and D. Quirion, *Doubled Full Shot Noise in Quantum Coherent Superconductor-Semiconductor Junctions*, Phys. Rev. Lett. **90**, 067002 (2003).

[28] R. de Picciotto, M. Reznikov, M. Heiblum, V. Umansky, G. Bunin and D. Mahalu, *Direct observation of a fractional charge*, Nature **389**, 162 (1997).

[29] H. Nyquist, *Thermal Agitation of Electric Charge in Conductors*, Phys. Rev. **32**, 110 (1928).

[30] J. Johnson, *Thermal Agitation of Electricity in Conductors*, Phys. Rev. **32**, 97 (1928).

[31] H.B. Callen and T.A. Welton, *Irreversibility and Generalized Noise*, Phys. Rev. **83**, 34 (1951).

[32] R. Kubo, *The fluctuation-dissipation theorem*, Rep. Prog. Phys. **29**, 255 (1966).

[33] N. Cherroret and S.E. Skipetrov, *Long-Range Correlations of Density in a Bose-Einstein Condensate Expanding in a Random Potential*, Phys. Rev. Lett. **101**, 190406 (2008).

[34] E. Altman, E. Demler and M. Lukin, *Probing many-body states of ultracold atoms via noise correlations*, Phys. Rev. A **70**, 013603 (2004).

[35] C. Ciuti, *Viewpoint: Statistical Flickers in a Bose-Einstein Condensate of Photons*, Physics **7**, 7 (2014).

[36] H.T.C. Stoof, K.B. Gubbels and D.B.M. Dickerscheid, *Ultracold Quantum Fields*, Springer (2009).

[37] G. Baym and C.J. Pethick, *Ground-State Properties of Magnetically Trapped Bose-Condensed Rubidium Gas*, Phys. Rev. Lett. **76**, 6 (1996).

[38] R.A. Nyman, M.H. Szymanska, *Interactions in dye-microcavity photon condensates and the prospects for their observation*, arXiv:1308.3588 [quant-ph] (2013).

[39] R.Y. Chiao, T.H. Hansson, J.M. Leinaas and S. Viefers, Phys. Rev. A. **69**, 063816 (2004).

[40] S. Yaltkaya and R. Aydin, *Experimental investigation of temperature effect on the refractive index of dye laser liquids*, Turk. J. Phys. **22**, 41 (2002).

[41] *Handbook of Chemistry and Physics*, CRC Press, 91st Edition (2009).

[42] A.-W. de Leeuw, H.T.C. Stoof and R.A. Duine, *Schwinger-Keldysh theory for Bose-Einstein condensation of photons in a dye-filled optical microcavity*, Phys. Rev. A **88**, 033829 (2013).

[43] R.R. Birge, *Kodak Laser Dyes*, Kodak publication JJ-169 (1987).

[44] J.R. Lakowicz, *Principles of fluorescence spectroscopy*, Springer (2006).

[45] J. Bardeen, L.N. Cooper and J.R. Schrieffer, *Theory of Superconductivity*, Phys. Rev. **108**, 1175 (1957).

[46] D.A. Kirzhnits and A.D. Linde, *Macroscopic consequences of the Weinberg model*, Phys. Lett. B **42**, 471 (1972).

[47] Y. Aoki, Z. Fodor, S.D. Katz and K.K. Szabó, *The QCD transition temperature: Results with physical masses in the continuum limit*, Phys. Lett. B **643**, 46 (2006).

[48] F. Karsch, *Transition temperature in QCD with physical light and strange quark masses*, J. Phys. G **34**, S627 (2007).

[49] L. Landau, *Theory of phase transformations*, Zh. Eksp. Teor. Fiz **7**, 19 (1937).

[50] Y. Nambu and G. Jona-Lasinio, *Dynamical Model of Elementary Particles Based on an Analogy with Superconductivity*, Phys. Rev. **122**, 345(1961).

[51] J. Goldstone, *Field Theories with Superconductor Solutions*, Nuovo Cim. **19**, 154 (1961).

[52] W. Heisenberg, *Zur Theorie der Ferromagnetismus*, Zeits. f. Physik **49**, 619 (1928).

[53] M. Lewenstein and L. You, *Quantum Phase Diffusion of a Bose-Einstein Condensate*, Phys. Rev. Lett. **77**, 3489 (1996).

[54] A. Imamo$\bar{\text{g}}$lu, M. Lewenstein and L. You, *Inhibition of Coherence in Trapped Bose-Einstein Condensates*, Phys. Rev. Lett. **78**, 2511 (1997).

[55] S.Yi, Ö.E. Müstecaplioğlu and L. You, *Quantum Phase Diffusions of a Spinor Condensate*, Phys. Rev. Lett. **90**, 140404 (2003).

[56] J. Javanainen and M. Wilkens, *Phase and Phase Diffusion of a Split Bose-Einstein Condensate*, Phys. Rev. Lett. **78**, 4675 (1997).

[57] K. Mølmer, *Phase collapse and excitations in Bose-Einstein condensates*, Phys. Rev. A **58**, 566 (1998).

[58] R. Graham, *Decoherence of Bose-Einstein Condensates in Traps at Finite Temperature*, Phys. Rev. Lett. **81**, 5262 (1998).

[59] H. Xiong, S. Liu, G. Huang and L. Wang, *Phase diffusion of BoseEinstein condensates in a one-dimensional optical lattice*, J. Phys. B **36**, 3315 (2003).

[60] M.R. Andrews, C.G. Townsend, H.-J. Miesner, D.S. Durfee, D.M. Kurn and W. Ketterle, *Observation of Interference Between two Bose Condensates*, Science **275**, 637 (1997).

[61] D.S. Hall, M.R. Matthews, C.E. Wieman and E.A. Cornell, *Measurements of Relative Phase in Two-Component Bose-Einstein Condensates*, Phys. Rev. Lett. **81**, 1543 (1998).

[62] A. Altland and B. Simons, *Condensed Matter Field Theory*, Cambridge University Press (2010).

[63] M. Greiner, O. Mandel, T.W. Hänsch and I. Bloch, *Collapse and revival of the matter wave field of a BoseEinstein condensate*, Nature **419**, 51 (2002).

[64] H.T.C. Stoof, *Coherent versus Incoherent Dynamics during Bose-Einstein Condensation in Atomic Gases*, J. Low Temp. Phys **114**, 11 (1999).

[65] R.A. Duine and H.T.C. Stoof, *Stochastic Dynamics of a Trapped Bose-Einstein Condensate*, Phys. Rev. A **65**, 013603 (2001).

[66] M. Abbarchi, A. Amo, V.G. Sala, D.D. Solnyshkov, H. Flayac, L. Ferrier, I. Sagnes, E. Galopin, A. Lemaître, G. Malpuech and J. Bloch, *Macroscopic quantum self-trapping and Josephson oscillations of exciton polaritons*, Nature Physics **9**, 275 (2013).

[67] K.G. Lagoudakis, B. Pietka, M. Wouters, R. André, B. Deveaud-Plédran, *Coherent Oscillations in an Exciton-Polariton Josephson Junction*, Phys. Rev. Lett. **105**, 120403 (2010).

[68] K. Madison, F. Chevy, W. Wohlleben, J. Dalibard, *Vortex Formation in a Stirred Bose-Einstein Condensate*, Phys. Rev. Lett. **84** , 806 (2000).

[69] D. Guéry-Odelin and S. Stringari, *Scissors mode and superfluidity of a trapped Bose-Einstein condensed gas*, Phys. Rev. Lett **83**, 4452 (1999).

[70] H.T.C. Stoof and D. van Oosten, *Shaping the Sound of Light*, FOM Projectruimte (2014).

[71] C. M. Wilson, G. Johansson, A. Pourkabirian, M. Simoen, J.R. Johansson, T. Duty, F. Nori, P. Delsing, *Observation of the dynamical Casimir effect in a superconducting circuit*, Nature **479**, 376 (2011).